

**MECHANICAL CHARACTERIZATION OF PFSA
MEMBRANE IN FUEL CELL**

by
Jun Qian

A thesis submitted to the Faculty of the University of Delaware in partial fulfillment of the requirements for the degree of Master of Science in Mechanical Engineering

Winter 2019

© 2019 Jun Qian
All Rights Reserved

**MECHANICAL CHARACTERIZATION OF PFSA
MEMBRANE IN FUEL CELL**

by

Jun Qian

Approved: _____
Michael H. Santare, Ph.D.
Professor in charge of thesis on behalf of the Advisory Committee

Approved: _____
Ajay Prasad, Ph.D.
Chair of the Department of Mechanical Engineering

Approved: _____
Levi T. Thompson, Ph.D.
Dean of the College of Engineering

Approved: _____
Douglas J. Doren, Ph.D.
Interim Vice Provost for Graduate and Professional Education

ACKNOWLEDGMENTS

I would like to thank all the people who have helped me throughout my stay at University of Delaware and people contributed to this thesis.

I would like to express my sincere gratitude to my advisor Dr. Michael H. Santare and Dr. Anette M. Karlsson for their continuous support and guidance throughout my study in their group. They have provided me a great academic environment allowing me to explore deep in the academic field. They also offered me great help when I encounter problems. Their help in improving my presentation and writing techniques is also appreciated.

I would like to thank Dr. Robert L. Opila from Department of Material Science and Engineering for serving my dissertation committee and reviewing my thesis.

I would like to acknowledge the support from all my lab mates. Thanks to Dr. Zongwen Lu for guidance on the experimental design and performance. Thanks to Dr. Narinder S. Khattrra and Dr. Guoliang Ding for their support on numerical modeling. I am grateful to Dr. Ahmet Kusoglu from Lawrence Berkeley National Laboratory for sharing tests techniques through discussions.

Many thanks go to department coordinators Lisa Katzmire and Letita Toto for helping from time to time and thanks to the lab coordinator Roger Stahl for his help.

Lastly, I would thank my wife for your continuous support to accomplish my degree.

TABLE OF CONTENTS

LIST OF TABLES	vi
LIST OF FIGURES	vii
ABSTRACT	ix
Chapter	
1 INTRODUCTION	1
1.1 Proton Exchange Membrane Fuel Cell.....	1
1.2 Perfluorosulfonic Acid Membrane	3
1.3 Fatigue Investigation of the Nafion® Membrane.....	6
1.4 Objectives and Outlines.....	8
2 FATIGUE INVESTIGATION OF THE NAFION® MEMBRANE	9
2.1 Overview	9
2.2 Experiment Facilities and Test Setup	11
2.3 Test Control Mode.....	13
2.3.1 Displacement Control Mode.....	13
2.3.2 Force Control Mode	14
2.4 Results and Discussion	16
2.5 Summary.....	19
3 INVESTIGATION OF SWELLING IN THICKNESS DIRECTION	20
3.1 Overview	20
3.2 Experimental Investigation.....	21
3.2.1 Experiment Facilities.....	21
3.2.2 Test Procedure	23
3.2.3 Results and Discussion	25
3.3 Numerical Investigation	30
3.3.1 Overview	30

3.3.2	Description of the Model.....	31
3.3.2.1	Out-of-plane Model	31
3.3.2.1.1	Assumptions	32
3.3.2.1.2	Boundary Conditions.....	32
3.3.2.2	In-plane Model	34
3.3.2.2.1	Assumptions	35
3.3.2.2.2	Boundary Conditions.....	35
3.3.3	Material Properties	36
3.3.4	Results	37
3.4	Mechanical Response of PFSA Membranes under Hygrothermal Loading in Fuel Cell.....	43
3.4.1	Material Properties	45
3.4.2	Assumptions	45
3.4.3	Boundary Condition	46
3.4.4	Results and Discussion.....	47
3.5	Summary.....	55
4	CONCLUSIONS AND FUTURE WORK.....	57
4.1	Summary of Work	57
4.2	Future Considerations.....	59
	REFERENCES	62

LIST OF TABLES

Table 2-1 Environmental Condition for Fatigue Tests.....	11
Table 3-1 (a) coefficient of in-plane swelling in terms of polynomial function [18]...	37
Table 3-1 (b) coefficient of out-of-plane swelling in terms of polynomial function ...	37

LIST OF FIGURES

Figure 1-1 Representation of PEM Fuel Cell System [29].....	2
Figure 2-1 Schematic of test configurations of Fatigue test on Nafion® 211 membrane with Pre-existing crack	10
Figure 2-2 Initiating the pre-existing crack	11
Figure 2-3 MTS testing system with custom designed environmental chamber.....	12
Figure 2-4 Experiment setup for the fatigue test	13
Figure 2-5 Force and displacement as a function of time for displacement-controlled fatigue loading of Nafion® 211 membrane at several Temp-RH.....	14
Figure 2-6 Force and displacement as functions of time for displacement-controlled fatigue loading of Nafion® 211 membrane at 100 and 1900 cycles.....	15
Figure 2-7 Cycles to failure for Nafion® 211 membrane as function of RH for T=45°C with nominal mean stress of 4.76 MPa and amplitude of 2.38 MPa	17
Figure 2-8 Cycles to failure for Nafion® 211 membrane as a function of T for various RH with nominal mean stress of 4.76 MPa and amplitude of 2.38 MPa	17
Figure 2-9 Cycles to failure for Nafion® 211 membrane as a function of T and nominal mean stress for RH=50%.....	18
Figure 3-1 Thermo Mechanical Testing System with (a) Control system and Furnace b) Loading probe and stage	22
Figure 3-2 V-gen Humidity Generator	23
Figure 3-3 (a) Thickness change of Nafion® 212 membrane in the thickness direction due to temperature and humidity change (A successful test)...	27

Figure 3-3 (b) Thickness change of Nafion® 212 membrane in the thickness direction due to temperature and humidity change (A failed test)	27
Figure 3-4 Comparison between In-plane and Out-of-plane of thickness change due to humidity variation at both 30°C and 80°C	29
Figure 3-5 Swelling coefficient of PFSA membrane under various temperature and humidity combination.....	29
Figure 3-6 Schematic of numerical model for out-of-plane swelling coefficients investigation	31
Figure 3-7 An Example of temperature and humidity cycle in the simulation	34
Figure 3-8 Schematic of numerical model for in-plane swelling coefficients investigation	35
Figure 3-9 (a) Stress distribution in membrane under hygrothermal loading F=14.13N with three friction coefficients a) F=0, b) F=.2, c) F=.4	39
Figure 3-9 (b) Simulated out-of-plane displacement for model shown in Figure 3-6; Load=0.06N and with three friction coefficients	39
Figure 3-9 (c) Simulated out-of-plane displacement for model shown in Figure 3-6; Load=14.13N three friction coefficients	40
Figure 3-10 In-plane swelling using model Figure 3-8.....	41
Figure 3-11 out-of-plane swelling using model Figure 18b.....	42
Figure 3-12 Schematic of the 2D generalization of fuel cell unit [32].....	44
Figure 3-13 Development of the stress for elements in the membrane at the groove and the land side	47
Figure 3-14 In-plane stress distribution contours (A-E) in the membrane during the first cycle of Gore™ RH load profile.....	50
Figure 3-15 Evolution of the in-plane stress at Groove Side	53
Figure 3-16 Evolution of the in-plane stress for isotropic and anisotropic case	54

ABSTRACT

The durability of Proton Exchange Membrane Fuel Cells (PEMFCs) has been a critical obstacle that inhibits the commercialization of fuel cells while the durability of the PFSA membrane often determines the lifetime of the fuel cell. Both mechanical and chemical factors contribute to the failure of the fuel cell unit. Mechanical stresses developed due to changes in the temperature and relative humidity causing deformation during the fuel cell operation which in turn contributes to the mechanical damage. This work is aimed at understanding the mechanical response of the membrane under hygrothermal loading. Fatigue testing was performed to characterize and understand the fatigue behavior of the membrane and its dependence on the environmental conditions. Also, the out-of-plane hygrothermal swelling of the membrane was measured and found to be different than the in-plane swelling. The anisotropy of the swelling coefficients is incorporated in a numerical model to investigate the development of stresses in the membrane in an operating fuel cell stack.

Fatigue tests were performed on Nafion® 211 membrane to understand the failure mechanism and to predict the lifetime of the membrane. Both mechanical and hygrothermal load have an influence on the fatigue life of PFSA membrane. These tests showed that fatigue life of the membrane decreases with an increase in stress. The fatigue life decreases exponentially with the relative humidity at given temperature and stress. When the humidity and stress are constant, the fatigue life decreases substantially with increasing the temperature. Moreover, when the

temperature and relative humidity are below a certain limit (i.e. $T=25\text{C}$ $\text{RH}=50\%$) for a selected mechanical load, the fatigue crack in the membrane stops propagating or propagates at a significantly small rate, which make the membrane seem to have a fatigue limit under these conditions.

The out-of-plane swelling behavior of the membrane was measured as a function of hygrothermal loading. The results show that the swelling of the membrane under hygrothermal loading is not isotropic as previously assumed. In the out-of-plane direction, the swelling of the membrane increases with increasing relative humidity but decreases with increasing temperature. The swelling coefficient in this direction is larger than that in the in-plane direction for almost all temperatures, but the difference is more significant when the temperature is low. The out-of-plane and in-plane swelling behaviors are described using separate polynomial equations and incorporated into a fuel cell numerical model. Considering the anisotropy of the swelling of the membrane relative to the isotropic model, the stress distribution and stress history in the fuel cell changes significantly but the spot where maximum compressive and tensile stress occur remains the same. However, the magnitude of the stress increases. For the GoreTM cycle, the stress range increases by 13.2% and the maximum residual tensile stress increases by 11.2%. For DoE RH cycle, the stress range increases by 12.4% and the maximum residual tensile stress increases by 9.2%. This result indicates that the lifetime prediction from the isotropic model might be longer than when the swelling anisotropy in the membrane is considered.

Chapter 1

INTRODUCTION

1.1 Proton Exchange Membrane Fuel Cell

Fuel cell technology, which was first introduced over 160 years ago [1], converts chemical energy to electrical energy through a direct chemical reaction without combustion. Compared with the traditional internal combustion engine, which mostly relies on fossil fuels as the power source, the fuel cell has zero emissions but higher energy density and higher efficiency [2], so it can be a good alternative energy resource for power plants, automobile industries and portable devices.

Researchers have developed several types of fuel cell systems and each type of the fuel cell has its own advantages, thus having different potential applications [3]. The proton exchange membrane fuel cells (PEMFCs) have the capability to provide a power source for transportation and stationary applications with hydrogen as fuel [4]. The system runs at relatively low temperature, therefore it takes a short time to startup and shut down. Meanwhile, the PEM fuel has high potential energy density and high energy efficiency. As a result, the PEM fuel cells can be widely used ranging from portable to large-scale power sources, especially in automobile industry. In recent years, major automobile manufacturers introduced several models of fuel cell vehicles into the market. In 2014, Hyundai firstly introduced a fuel cell vehicle named Tucson. In 2015, Toyota followed into the market by introducing its fuel cell car Mirai and in 2016 Honda produced a fuel cell powered vehicle with the name Clarity.

In a typical PEM fuel cell, the fuel is supplied in the form of hydrogen to the anode side through the gas diffusion layers (GDLs). The hydrogen molecule is split into protons and electrons at the anode side. On the cathode side of the fuel cell, the oxygen contained in the air is supplied and is combined with the protons and electrons coming from the anode to generate water and heat (Figure 1-1). The proton exchange membrane (PEM), which is coated platinum particles, is sandwiched between gas diffusion layers. The membrane insulates against electron flow and allows only positive ions (protons) to pass through. Therefore, a voltage is formed between the electrodes. The membrane also functions as a gas barrier to prevent the direct reacting of oxygen and hydrogen.

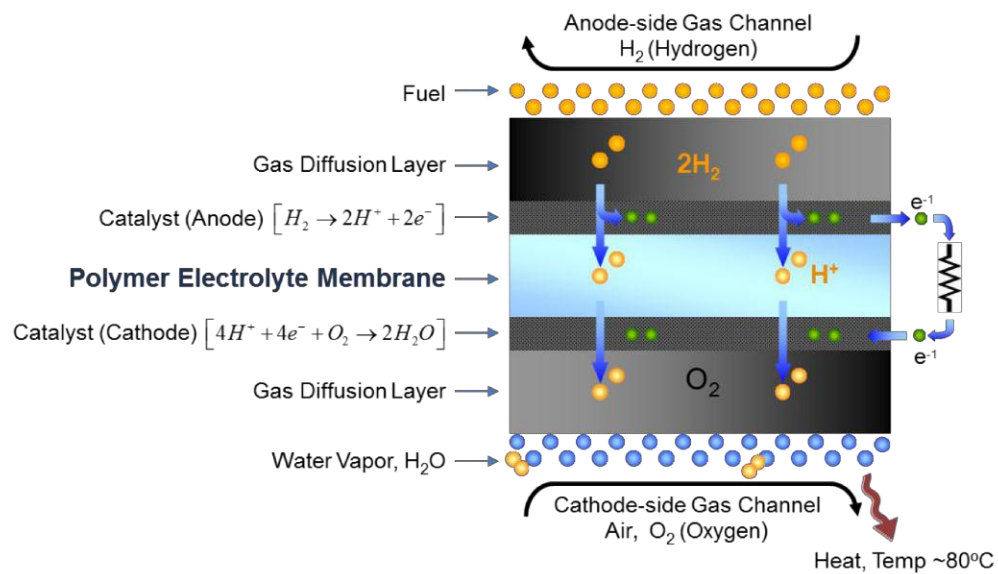


Figure 1-1 Representation of PEM Fuel Cell System [29]

However, one of the key factors that have limited the commercialization of PEMFCs is the durability of the cell components [5]. In 2015, the Department of Energy of the United States set the target of increasing automotive fuel cell durability from 2500h (75,000 miles equivalent) to 5000h (150,000 miles equivalent) by 2020 [3]. And more research effort is needed to extend the lifetime of PEMFCs. According to the previous research, the failure of PEMFCs is mainly due to the failure of the PEM, which is driven by both chemical degradation and mechanical damage [7-13]. The chemical degradation has been researched by other researchers [14-15] but we believe the mechanical factors are also important in determining the lifetime of PEMFCs. In a typical fuel cell operation, the membrane undergoes hygrothermal cycles because of the production of water and heat at the electrode. The membrane expands and swells when the temperature and humidity go up and compressive stresses are induced because of the constraint from other cell components [16]. When the compressive stress goes beyond the yield stress, plastic or permanent deformation can occur. When temperature and humidity reduce, the membrane shrinks, causing residual in-plane tensile stress in the membrane. This compressive and tensile stress cycling drives the initiation and propagation of cracks in the membrane. When a crack propagates a substantial distance through the membrane, the fuel cell efficiency drops until the cell is deemed to have failed [17-26].

1.2 Perfluorosulfonic Acid Membrane

Perfluorosulfonic acid (PFSA) ionomer is one of the most widely used electrolyte materials in PEMFCs industry. In the 1970s, DuPont introduced a

membrane of PFSA ionomer, the Nafion® membrane. And Nafion® membrane soon becomes the benchmark among available commercial PFSA materials. Other advanced perfluorosulfonic acid membranes are also introduced in the market by companies such as Dow, Asahi Chemical Industry (Asiplex™) and W. L. Gore and Associates, Inc. (Gore-Select™) [27-29].

As the core component of the fuel cell, the membrane should have high proton conductivity and zero electron conductivity to ensure the high electronic efficiency. Meanwhile, the membrane should also have sufficient mechanical strength to ensure the stability of the fuel cell. In recent years, significant effort has been placed in investigating the mechanical response of membrane by means of experiments and simulation [16-23]. Cleghorn et al. [7] concluded that absorption of water in the membrane significantly decreases the membrane strength due to the plasticization of the ionomer. Tang et al. [21] tested the material properties of Nafion® 112 membrane in tension at various temperature and humidity conditions. They showed that the elastic modulus and proportional limit of the membrane decrease with increasing temperature and humidity. The work also showed that when the temperature is higher, the membrane has a higher swelling coefficient. Lu et al. [30, 33, 39] extended the above work by considering the time dependence of the material properties, measured by running the tensile test under two different strain rates and conducting stress relaxation experiments. The results show that both the stiffness and the proportional limit increase with the strain rate. Goulet et al. [43] show a great difference in the mechanical properties of plain PFSA membranes and the catalyst (mostly platinum) coated membranes. They found that PFSA membrane alone, can generate twice as

much residual in-plane stress than the catalyst coated membranes during dehydration [44].

On the modeling side, Weber et al. [31] used a one-dimensional model to incorporate the mechanical properties of PFSA membrane in a fuel cell model to predict the water transport and swelling of Nafion® membrane. They concluded that the mechanical constraints influence the membrane water content as well as the electrochemical performance. Tang et al. [17-18] developed a numerical model to represent fuel cell operation by assuming the membrane is an isotropic linear-elastic material. In their model, the elastic modulus and swelling coefficients were taken as constants during hygrothermal cycles. Kusoglu et al. [16] extended with this work by modifying the model to include linear-elastic, perfectly-plastic property of the membrane and included the mechanical properties as functions of temperature and water content. Kusoglu et al. [19] then further extended the work by describing the membrane with linear elastic-plastic behavior and isotropic hardening material properties. Solasi et al. [34] employed a nonlinear model to capture the time dependent hygrothermal behavior of membranes. Khattra et al. [32] developed a visco-elastic plastic model to investigate the constitutive response of the membrane. The parameters in the model are obtained by tensile and stress-relaxation experiments [26, 33]. Silberstein et al. [35, 38, 56] extended the model by adding a back stress to the visco-plastic element to better capture unloading behavior in cyclic loading conditions. In their model, a micro-mechanical constitutive model is utilized to capture the stress development in the membrane under monotonic and cyclic loading.

1.3 Fatigue Investigation of the Nafion® Membrane

Failure mechanisms of the membrane have been studied by Lai et al. [36], Kusoglu et al. [16, 40, 41] and Weber et al. [31]. It has been shown that compressive and tensile stresses induced by hygrothermal cycles are critical to the mechanical damage of the membrane. The water and heat generated during the fuel cell operation lead to swelling and shrinkage of the membrane, resulting in cyclic stresses and strain since the membrane is constrained by other components in the fuel cell stack. And the stress and strain can further induce fatigue that can initiate cracks at locations where the stress is large [36, 16].

Burlatsky et al. [68] introduced a theoretical model to investigate the durability of PFSA membranes under humidity loading cycles. There are three components of the model: The first component is developed to correlate the relative humidity in the fuel channels to the applied relative humidity and operating time. The second component in this model relates the stress distribution in the membrane to the applied humidity profile. The third component is used to predict the lifetime of the PFSA membrane by considering the experiment data of membrane under stress cycles. With the three models mentioned above, Burlatsky et al. [68] investigated the influence of relative humidity changes at the cathode side on the number of cycles that a membrane can run before failure during the fuel cell operation.

Aindow et al. [37] conducted ex-situ fatigue tests on Nafion® membrane by applying mechanical cyclic loading to study the membrane's resistance to mechanical failure under various humidities. Khorasany et al. [45] conducted ex-situ experiments to study the failure mechanism of membrane. They performed tests with dog bone-shaped samples under cyclic mechanical loading to study the fatigue characterization

of the PFSA membrane. They found mechanical stress, temperature, and relative humidity all have influences on the time for a crack to be initiated. They also found that the temperature has a relatively more significant effect than relative humidity. Y. Singh, et al. [42] performed ex-situ experiments to test the crack propagation rate of Nafion® 211 membranes under different combination of stress, temperature and relative humidity. They found the stress intensity has a strong influence on the crack propagation rate. Qiang et al. [70] investigated the fatigue crack propagation rates under different loading mechanical/hygrothermal conditions and studied the influence of transverse stress on the fatigue crack propagation rate. In Zhang's extended work [71], the crack propagation resistance in reinforced PFSA membrane was investigated and compared with the that of classic PFSA membrane. Their work shows how the reinforcement of the membrane impacts the fatigue crack growth rate of Nafion® XL membrane. Fatigue tests on the membrane electrode assembly (MEA) were conducted by Pestrak et al. [37] by using biaxial fatigue tests and by Kai et al. [38] using cyclic tensile loading. In Alavijeh's tensile fatigue-creep testing [60] on catalyst coated membranes, the fatigue-creep behavior is analyzed by putting the membrane under tensile and hygrothermal loading. The thermal expansion is measured on partially degraded specimens. Micro-structural characterization is used to evaluate the microstructural decay of the membrane. From their observations of the MEA surface during the fatigue testing, they concluded that cracks initiate in the catalyst layer after the MEA yields. These cracks can propagate into the membrane, which correlates with failure of the fuel cell. However, cracks in the catalyst layer alone, do not necessarily signal failure of the fuel cell. Although these studies lend insight, further investigation

of the fatigue behavior of membrane at various temperature and humidity could help to gain a deeper understanding of the durability in fuel cells.

1.4 Objectives and Outlines

The overall goal of this work is to further understand the material properties of the PFSA membrane and how they influence the mechanical response of the membrane in the fuel cell under hygrothermal loading. This will be done by means of a combination of experimental and numerical investigations. Two mechanical behaviors that are critical to the understanding of membrane durability, fatigue failure and swelling behavior, will be studied in this thesis.

In chapter 2, fatigue test protocols which have been developed in the preliminary research, will be used to perform tests to study the effect of cyclically applied load on the resistance to fatigue failure of the membrane under various environmental conditions.

Chapter 3 will focus on investigating the anisotropy of the membrane swelling behavior. Experiments are developed and conducted on a TMA (Thermo Mechanical Analyzer) [21] that together with numerical analysis, will be used to obtain the dimensional change of the membrane in the out-of-plane (thickness) direction, under hygrothermal loading and its dependence on temperature and humidity. The swelling coefficients in the out-of-plane direction, along with those already determined in the in-plane direction, are then incorporated into a 2-D finite element model of fuel cell unit to study the time-dependent mechanical response of membrane under different hygrothermal loading cycles.

Chapter 2

FATIGUE INVESTIGATION OF THE NAFION® MEMBRANE

2.1 Overview

In this part of the investigation, we conducted a study of the fatigue life of the pre-cracked membrane under various combinations of temperature and humidity conditions.

In the fatigue life tests, samples of PFSA membranes were investigated for fatigue failure under a range of environmental conditions (Table 1). The schematic of the test is shown in Figure 2-1. The specimen size 20 mm x 50 mm, is used in the current test to ensure the stress field near the crack tip is not affected by the stress induced by the grip. Prior to each test, the width of the specimen was measured with a caliper at three locations along the sample. The average of these three measurements was used, along with the calculated thickness (explained in chapter 3), as the nominal dimensions of the sample at ambient temperature and humidity. The sample was then aligned with the extension rod and clamped between two grips. The distance between the grip is then set to 50 mm before the membrane is fixed. A set of preliminary tests were performed to determine the test setups, including the crack length and frequency of the cyclic load. The material tested in these experiments is viscoelastic and when this type of material is subjected to a sinusoidal stress, the strain lags the stress by a phase angle, which is dependent on the frequency. In the current test, we selected 0.1Hz as the frequency because under this frequency the phase angle is small enough

to be neglected and at the same time, the total experiment time is not too long. The initial crack length is selected as 1mm (5% of the total width of the specimen) to ensure that the fatigue life of the pre-cracked specimen is measurable. A scalpel was used to initiate the crack which was immersed in liquid nitrogen before cutting the crack to ensure a repeatable, relatively sharp crack tip (Figure 2-2). The length and configuration of the crack on the specimens were measured and visually confirmed under a microscope before testing. Having established a reasonable range for testing parameters, tests can be conducted to determine the effects of the loading parameters (mean stress and stress amplitude) temperature and humidity on the fatigue life of the membrane.

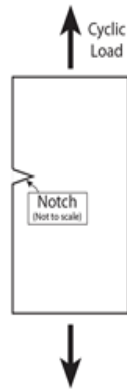


Figure 2-1 Schematic of test configurations of Fatigue test on Nafion® 211 membrane with Pre-existing crack

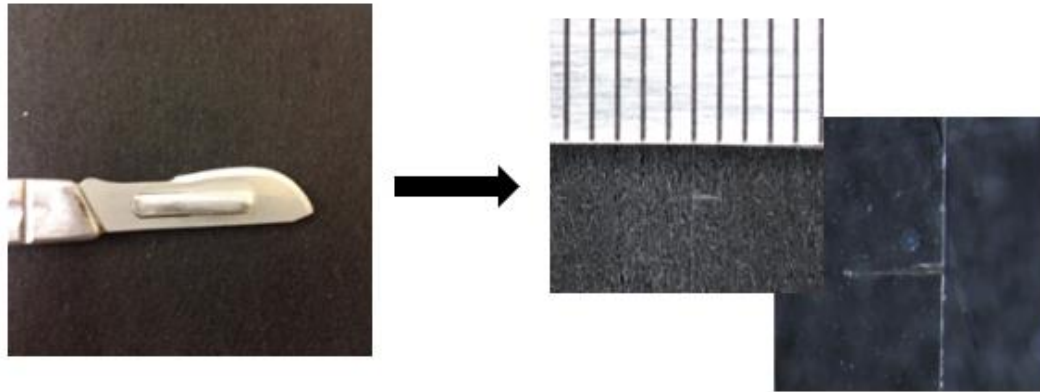


Figure 2-2 Initiating the pre-existing crack

2.2 Experiment Facilities and Test Setup

Temp/Relative Humidity	30%	40%	50%	60%	70%
25°C	x	x	x	x	x
35°C	x	x	x	x	x
45°C	x	x	x	x	x
55°C	x	x	x	x	x
65°C	x	x	x	x	x

Table 2-1 Environmental Condition for Fatigue Tests

The tests were performed in an MTS 858 Material Testing System with both static and dynamic loading capabilities. The testing system is fitted with a custom

designed environmental control chamber to run the experiments under the desired temperature and relative humidity. The testing system and chamber are shown in Figures 2-3. The sample is fixed by two grips and the load (displacement or force controlled) is applied through the extension rod at the top (Figure 2-4). For each test, the specimen was installed between the grips at room temperature and humidity with no preload. A negative displacement was set to ensure no mechanical load was applied before the membrane reached the equilibrium state. Then the temperature and humidity were set to the desired value and allowed at least one hour to let the membrane reach equilibrium. In each test, a cyclic mechanical stress was applied until the breakthrough of the specimen, which was considered to be the criterion for final failure. The frequency of the cyclic load was selected as 0.1 Hz. Each test is repeated 3 times for selected conditions to ensure reproducibility (Table 2-1).



Figure 2-3 MTS testing system with custom designed environmental chamber

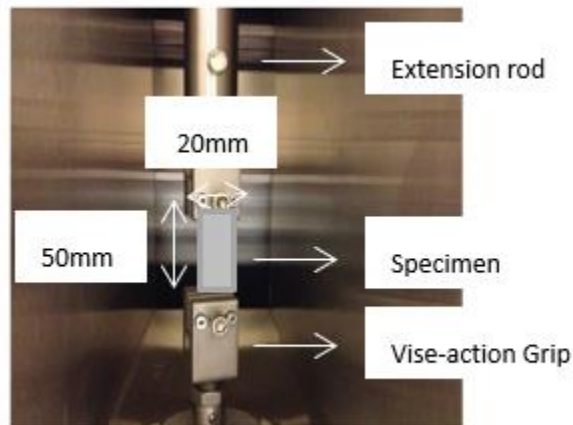


Figure 2-4 Experiment setup for the fatigue test

2.3 Test Control Mode

The equipment allows for two possible control modes available for the test, displacement and force control. Preliminary tests were conducted under both these two methods and results are compared.

2.3.1 Displacement Control Mode

The effects of temperature and humidity under the displacement control mode are shown in Figure 2-5. Figure 2-5 a, b and c show different environmental conditions, with the same uniform cyclic displacement loading (Amplitude=0.5mm-1.5mm). It can be seen from the figure that the stress decreases with time. It is also observed that with increasing temperature and humidity, the same displacement input results in smaller stress in the membrane.

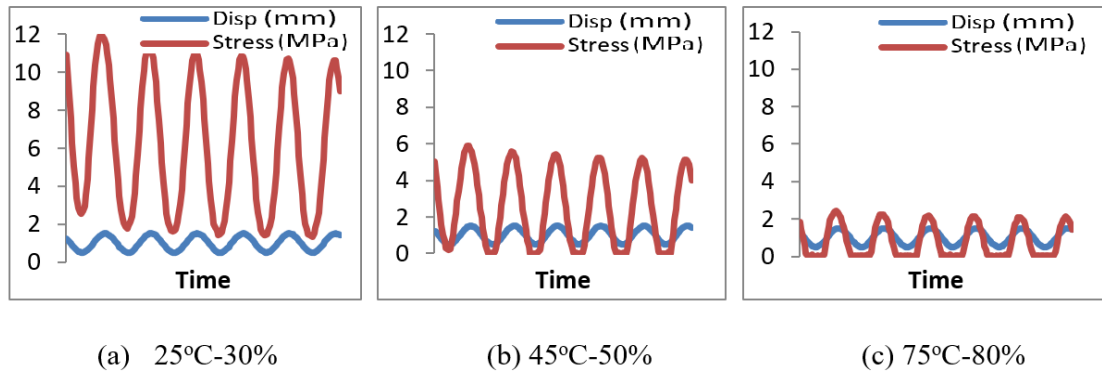


Figure 2-5 Force and displacement as a function of time for displacement-controlled fatigue loading of Nafion® 211 membrane at several Temp-RH

We can also see from Figure 2-5 b and Figure 2-5 c that the membrane goes slack (zero tensile stress) for part of the cycle, especially for the high temperature and humidity cases. While the membrane is slack, it will bend out-of-plane. The resulting stresses and deformations will be uncontrolled and unknown, resulting in an uncontrolled fatigue loading. To avoid this slacking behavior, a force-controlled testing is proposed.

2.3.2 Force Control Mode

From earlier results [39], the maximum tensile stress in the membrane during fuel cell operation is on the order of 10 MPa, which corresponds to 5.0 N load for a 20mm wide test specimen of Nafion® 211 membrane (with a pre-test thickness of 25.4 microns). This indicates the nominal load applied to a membrane with pre-

existing crack should be no more than 5.0 N to simulate conditions that are likely to be experienced in-situ.

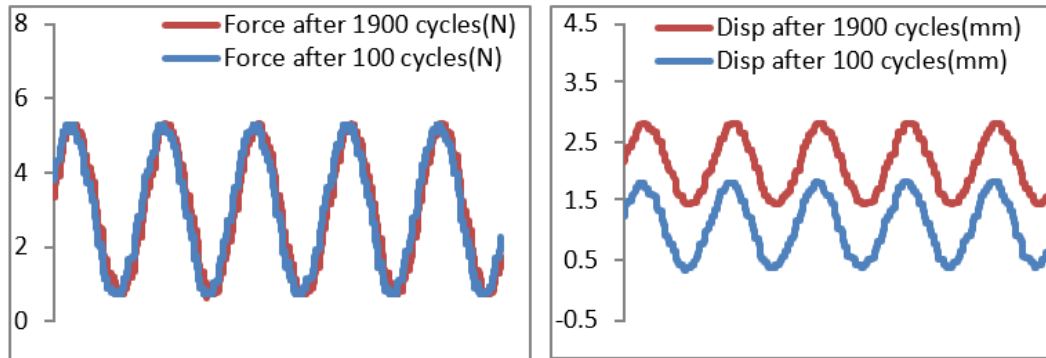


Figure 2-6 Force and displacement as functions of time for displacement-controlled fatigue loading of Nafion® 211 membrane at 100 and 1900 cycles

A sample test result for force control mode is shown in Figure 2-6. It can be seen from the figure that the membrane deforms significantly while the force level stays consistent. Also, due to the force-control, both force and displacement are larger than zero for the entire test. Compared with the displacement control mode, the load in the force control is stable and the displacement increases due to plastic deformation during the test. As a result, the force control mode is selected as the control method for the following test.

2.4 Results and Discussion

Investigation of the effect of relative humidity was conducted at fixed temperature ($T=45^{\circ}\text{C}$) and roughly fixed force level (nominal stress level). The results are shown in Figure 2-7. It is observed that with increasing relative humidity, the lifetime of the membrane decreases significantly. At high humidity (70%), the lifetime is only a few cycles. The effect of temperature on the fatigue life was also studied by setting a constant relative humidity ($\text{RH}=50\%$) and varying the temperature. Additional tests were conducted at higher relative humidity with the applied force level of Nominal Mean Stress=4.76 MPa and Nominal Stress Amplitude=2.38MPa. The results are shown in Figure 2-8. It can be observed that with an increase in relative humidity, the fatigue lifetime of Nafion® membrane decreases significantly. Also, at very high humidity, the fatigue lifetime is very low even when the temperature is relatively low.

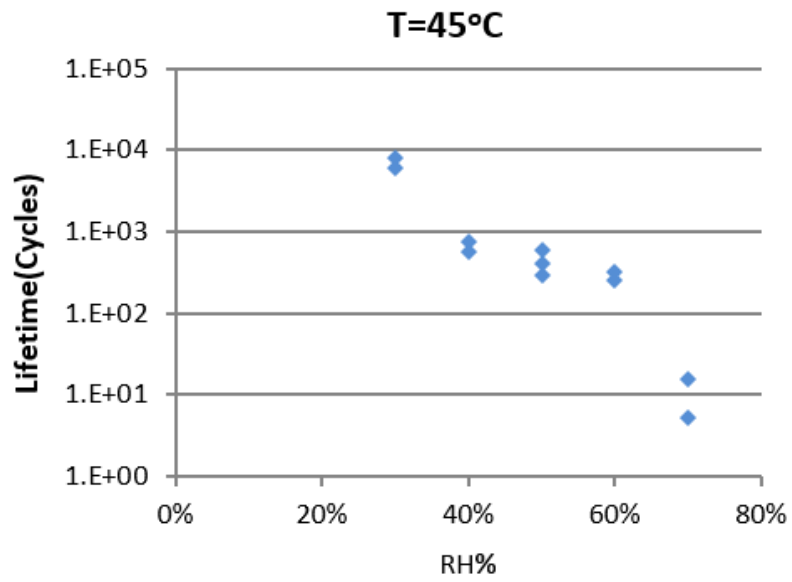


Figure 2-7 Cycles to failure for Nafion® 211 membrane as function of RH for T=45°C with nominal mean stress of 4.76 MPa and amplitude of 2.38 MPa

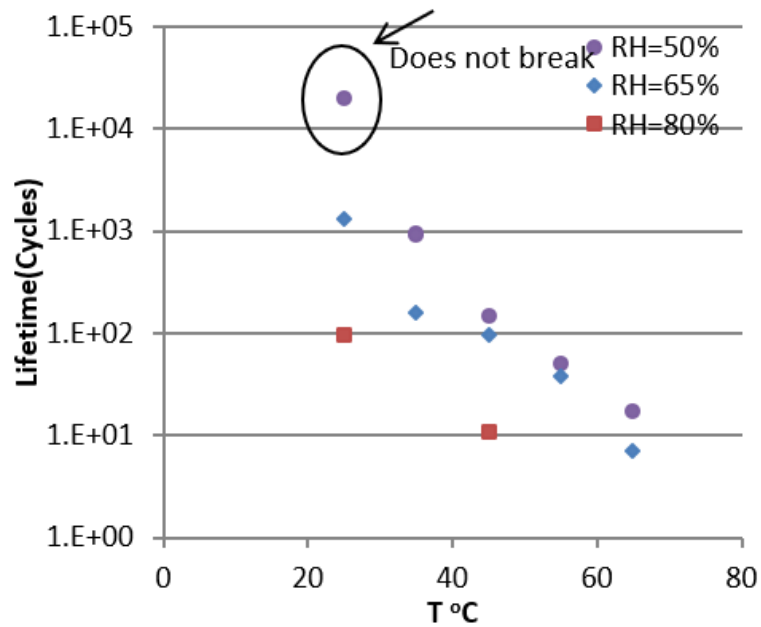


Figure 2-8 Cycles to failure for Nafion® 211 membrane as a function of T for various RH with nominal mean stress of 4.76 MPa and amplitude of 2.38 MPa

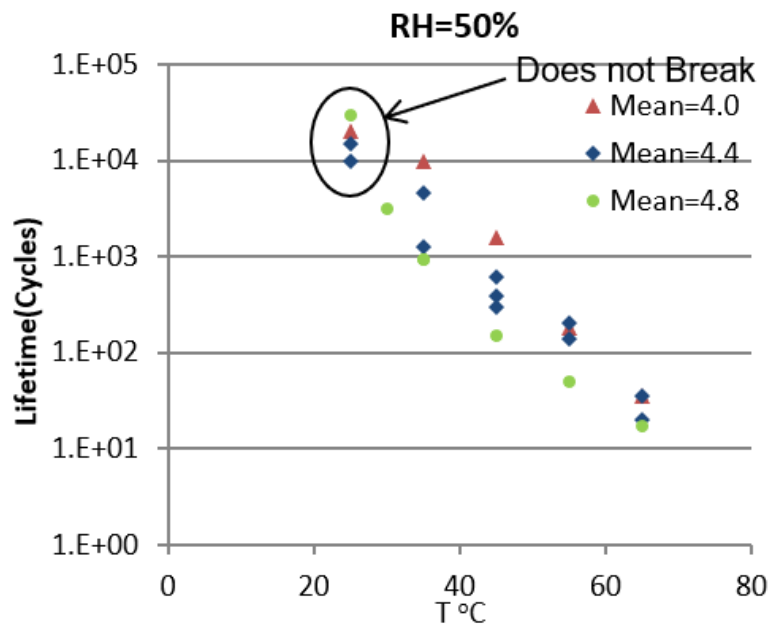


Figure 2-9 Cycles to failure for Nafion® 211 membrane as a function of T and nominal mean stress for RH=50%

In addition, various force levels were studied with constant force amplitude but different mean force values to investigate the effect of force level (nominal stress level). The results in Figure 2-9 show that with increasing temperature, the lifetime decreases logarithmically and this trend is observed for all the three force levels studied. Therefore, at a fixed temperature and humidity, increasing the mean stress while keeping force amplitude constant results in a decrease in cycles to failure.

2.5 Summary

Fatigue tests on the PFSA membrane Nafion® 211 membrane are performed in this work to understand the failure mechanism and predict the durability of the membrane. The test results reveal that both mechanical and hygrothermal load will have an influence on the fatigue life of PFSA membrane. Specifically, the fatigue life of the membrane decreases when the applied stress is larger. For a fixed mechanical load at a given temperature, the fatigue life decreases exponentially with the relative humidity, this is partly due to the difference in yield stress at these various humidity conditions. According to Lu's research [39], the proportional limit of the membrane decreases with increasing temperature or humidity, resulting in more plastic deformation at higher temperature or humidity, which leads to an earlier failure of the membrane. While at a given relative humidity, the fatigue life decreases substantially with increasing the temperature. This can be partly attributed to the fact that as the temperature goes up, the membrane has a smaller Young's modulus and proportional limit stress, making the material softer and more prone to plastic deformation which can lead to a shorter fatigue life of the membrane. Based on observations mentioned above, the fatigue life of the membrane increases with decreasing the temperature and relative humidity when the mechanical load is kept constant throughout the test. This is in accordance with our fatigue life test results. Moreover, we also observe that the temperature and relative humidity decreases below a certain level at a given load, for example, $T=25^{\circ}\text{C}$ $\text{RH}=50\%$ under our selected mechanical load, the crack in the membrane stops propagating or propagates at a significantly small rate, which make the membrane seems to have an "infinite" lifetime.

Chapter 3

INVESTIGATION OF SWELLING IN THICKNESS DIRECTION

3.1 Overview

The in-plane, time-dependent mechanical properties of the membrane materials, including Young's Modulus, yield stress and swelling coefficient have been determined through extensive experimentation previously conducted in our lab [25] [26] [33]. Numerical models of a typical unit of a fuel cell were developed to investigate the mechanical stresses in the membrane in a fuel cell under hygrothermal cycles using the material properties obtained from the experiments [32]. In these models, the out-of-plane properties are estimated from the in-plane data. However, to better capture the mechanical response of fuel cell and better interpret how the temperature and humidity influence the stresses in the membrane, more accurate out-of-plane properties need to be determined as well.

Swelling of the membrane during hydration is the driving force that induces stress in the membrane, so introduction of the swelling into the numerical model is a key to understanding the failure mechanisms of the fuel cell. However, due to a lack of data in our previous simulations, we have assumed that the swelling and mechanical properties of the unreinforced membrane are isotropic. But this assumption may not be accurate based on our preliminary experimental data. In addition, it may be less accurate for reinforced materials [19]. As a result, a set of tests measuring the dimensional change in the thickness direction is needed to obtain the out-of-plane

swelling coefficient under various environmental conditions. This swelling coefficient can be incorporated in the numerical models to better simulate the mechanical behavior and failure mechanisms of the fuel cell membrane.

The objective of the research proposed here is to understand how the PFSA membrane swells in the out-of-plane direction under temperature and humidity changes. Experiments will be conducted on TMA (Thermo Mechanical Analyzer) to investigate the dimensional change along the thickness direction during changes in temperature and humidity.

3.2 Experimental Investigation

3.2.1 Experiment Facilities

The thickness change due to temperature and humidity variation will be measured using a modified TA Instrument's Q400™ Thermomechanical analyzer ("TMA") fitted with its macro-expansion probe. The configuration of a standard TMA is illustrated in Figure 3-1 (More details of the test procedure and data collected can be found in Kurkoski [55]). For a single thickness measurement, the specimen is placed on the cylindrical test stage and is subjected to a small, known load by the probe at the top (Figure 3-1 b) to ensure contact between the specimen and the probe. A heating furnace with temperature controller (shown in Figure 3-1 a) is provided in order to control the temperature of the test. During the test, the probe can only move vertically and is linked to a force generator, which can apply a controlled load to the specimen. Changes in thickness of the membrane, caused by changes in temperature and load, are detected by a differential transformer. The test stage and probe are made of quartz, which has a nearly-zero coefficient of thermal expansion in the range of test

conditions. The test stage and upper surface of the probe are aligned. In order to perform different types of testing, e.g. bending, indenting and compression, the probe and stage can be changed.

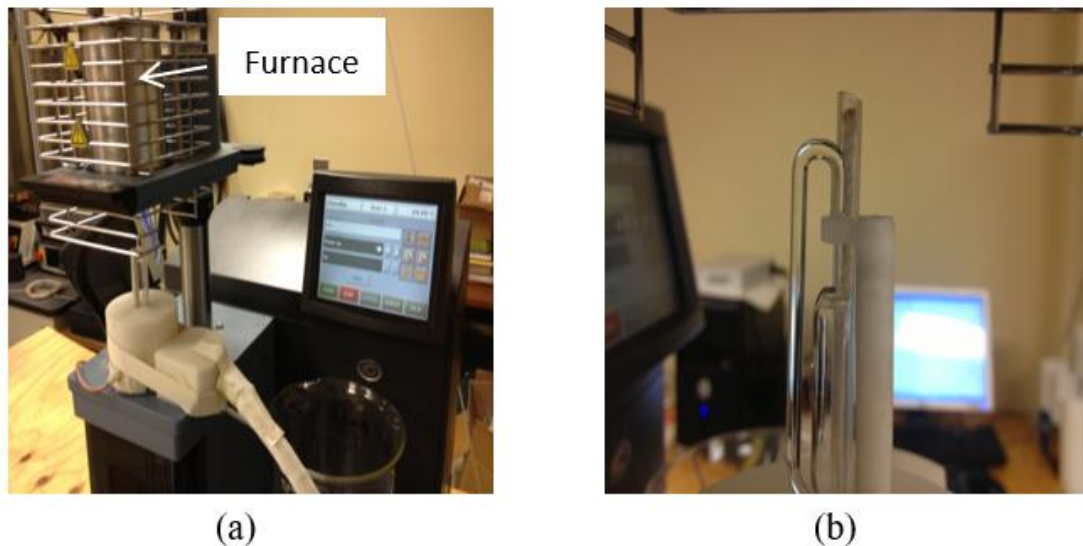


Figure 3-1 Thermo Mechanical Testing System with (a) Control system and Furnace
b) Loading probe and stage

The humidity in the test is controlled by a modification to the standard TMA that consists of a novel and versatile water vapor generation and calibration system consisting of an Instruquest V-Gen™ Model I Dew Point (V-gen) humidity generator and a humidity probe [55, 65]. The humidity generator uses the two-temperature principle to generate a stable dew point in the temperature range from 0 degrees to 80 degrees C. Therefore, the machine is theoretically capable of generating RH from 0 to 100% at those temperatures. The water vapor stream is generated in the V-gen and forced into the chamber through a plastic tube. A dry or semi-dry air source is

connected to the chamber through another plastic tube and the water vapor and dry air are combined to achieve the desired humidity. The water used for gas saturation is de-ionized and the supplied gas is dry air. A nylon wick is used to remove any condensed water from the tubing by the capillary effect [55]. Real-time data in the form of temperature, humidity and thickness is recorded by a computer connected to these two machines.



Figure 3-2 V-gen Humidity Generator

3.2.2 Test Procedure

Before each test, the load cell was calibrated with 3 weights (0g 50g and 100g). The input force was then assigned to the system. In the case of swelling measurements, a very low input force (0.06 N) was used in order to keep the

membrane from curling but not unduly compress the specimen. In preliminary testing, we found that Nafion® 212 membrane produced more repeatable results than Nafion® 211 membrane and therefore, Nafion® 212 membrane is used in the tests. Compared with the Nafion® 211 membrane that was used in the fatigue test, Nafion® 212 membrane is made from the same chemical formula and process but it is twice as thick (25.4 microns v. 50.8 microns). The thicker specimen is helpful to reduce the noise to signal ratio in the measured dimension. For each test case, the specimen was cut into a regular hexagon shaped piece with an approximate average diagonal of 6mm. The membrane was immersed in de-ionized water for 1 min to aid in removing the protective cover sheets on both sides. Then the membrane sample was carefully placed on the stage and the probe lowered. The thickness was checked to ensure that there was no wrinkling in the membrane and no bubbles between membrane and stage. For the purposes of calculating thickness change, the initial thickness of the membrane was obtained indirectly by subtracting the thickness of two cover sheets from the thickness of sample with the cover sheets on, measured prior to immersing in water. The reason for this is that the membrane absorbs water when removing the cover sheet and is then exposed in the ambient air, in which the humidity is uncontrolled. Therefore, the thickness of the sample when it is mounted in the TMA is not the thickness of dry membrane, but the thickness of membrane after absorbing some unmeasured quantity of water [55].

After the specimen was mounted, the furnace is moved into place and the V-gen was switched on. The furnace and dew point were adjusted until the temperature and humidity reached the desired starting points and were held constant. The thickness of the membrane was monitored until it stabilized under the constant temperature and

humidity. The dew point was then changed to achieve the desired final RH value, and again the thickness was monitored until it stabilized. The temperature, the initial and final humidities and the change in thickness were all recorded in real time.

3.2.3 Results and Discussion

The tests were conducted with the preload of 0.06N with various target temperature and humidity combinations. The humidity was adjusted to the starting value of 25% after raising the temperature to the desired value (30°C or 80°C in these cases). After the initial thickness stabilized, the dew point was changed to achieve the desired target relative humidity (50% or 75% in these cases). Two sample test measurements are shown in Figure 3-3 (a) and Figure 3-3 (b). Figure 3-3 (a) shows a good experimental result where we see that the thickness response quickly followed the humidity change. Notice that while the initial temperature was increased (approximately the first 15 minutes) the relative humidity in the test chamber decreased, which lead to an initial shrinkage of the membrane in the thickness direction. When the thickness stabilized at the initial temperature and humidity, water vapor was generated and forced into the chamber, which resulted in the increase of humidity. It can be observed that the thickness, again, increased rapidly with increasing humidity. However, it takes longer for the membrane thickness to reach steady state than the humidity. This is due to the fact that it takes some time for water to diffuse into the membrane especially with the probe covering most of the surface of the specimen. Figure 3-3 (b), however, shows a test result where equilibrium was never reached. In this test, the thickness does not change simultaneously with the

relative humidity (within the range of 0-20 minutes). This happened more frequently when the test temperature was higher. This could be due to the fact that at higher temperature, more water vapor is forced into the testing area resulting in some condensation in the system. Since both the water inlet and outlet are small in diameter, the condensed water could block the system, causing the relative humidity near the membrane to be quite different from the measured value in the chamber. Another problem seen in the test shown in Figure 3-3 (b) is that the relative humidity never reaches equilibrium throughout the test (20-360 minutes). This problem is frequently seen when the ambient relative humidity and test temperature is higher. This may also be caused by the condensed water mentioned above. As mentioned earlier in this chapter, a nylon wick is used to remove condensed water from the tubing by the capillary effect, but at higher relative humidity, this method may be ineffective.

To avoid the problems shown in Figure 3-3 (b), in the following tests, the relative humidity is changed slowly to prevent the liquid water from condensing in the test system. In addition, the tests are performed when the ambient relative humidity near the test facility is relatively low.

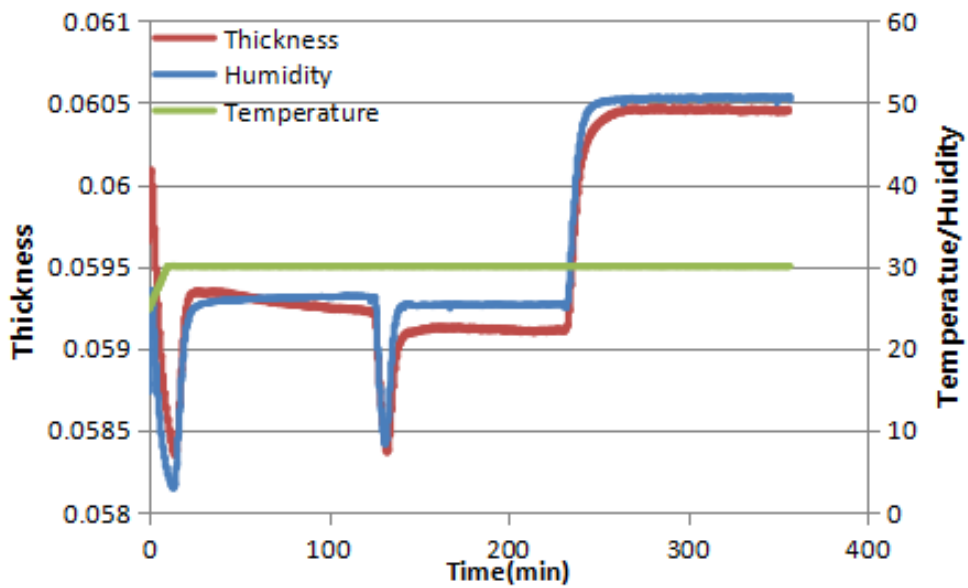


Figure 3-3 (a) Thickness change of Nafion® 212 membrane in the thickness direction due to temperature and humidity change (A successful test)

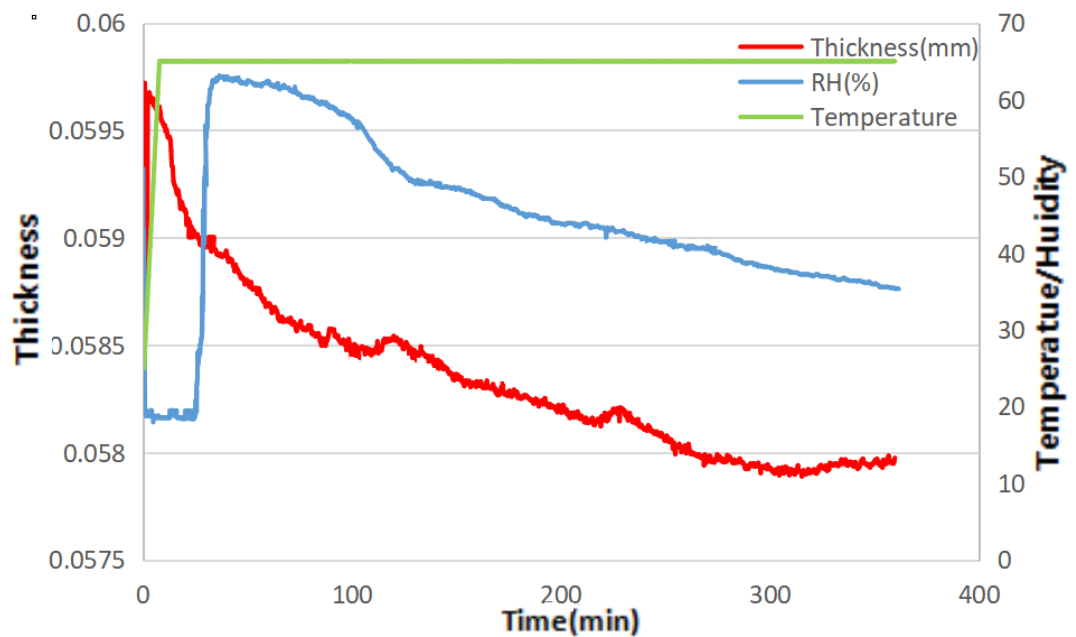


Figure 3-3 (b) Thickness change of Nafion® 212 membrane in the thickness direction due to temperature and humidity change (A failed test)

Several more tests were conducted at various temperature and humidity combinations. The test result shows little variation and good reproducibility, especially at the low temperature condition, where the desired relative humidity is relatively easy to achieve.

The dimensional change in the thickness direction, due to a change in environmental conditions, was also compared with the dimensional change in the in-plane direction. It has been shown that swelling in the machine direction shows little difference to that in the transverse direction [16], so here the comparison is made only between thickness direction and machine direction. The results are shown in Figure 3-4. It can be seen that the dimensional change at the thickness direction is more than that in the in-plane direction when the temperature is low. However, for the 80°C case, the result is the opposite: the dimensional change in the thickness direction is more in the in-plane direction. However, since a preload of 0.06N is applied to the membrane throughout the test and the dimensional change in such an experiment involves frictional and geometrical effects, the measured values cannot be directly interpreted as swelling strain. Therefore, numerical simulations were conducted and are presented in the following section to sort out these effects.

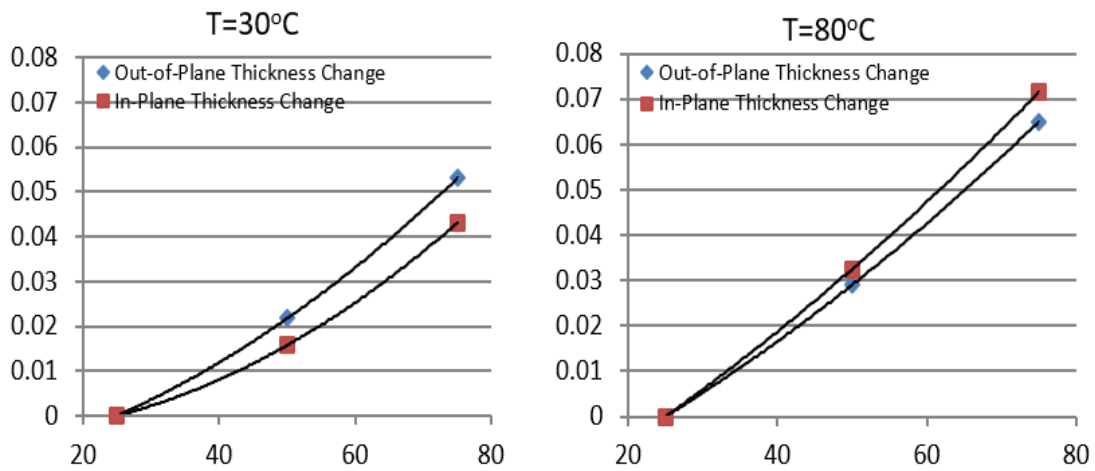


Figure 3-4 Comparison between In-plane and Out-of-plane of thickness change due to humidity variation at both 30°C and 80°C

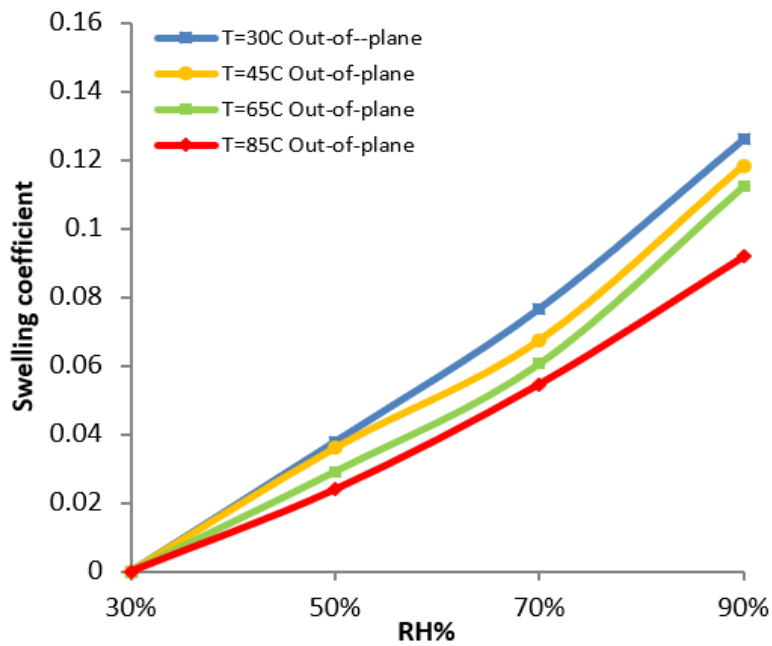


Figure 3-5 Swelling coefficient of PFSA membrane under various temperature and humidity combination

According to the results shown in Figure 3-5, the membrane expands with an increase in relative humidity at a given temperature. However, at the same humidity, when the temperature increases, the dimensional change decreases. This is an inverse relationship when compared with the in-plane direction swelling observed by Tang [16]. This indicates that the swelling behavior of PFSA membranes is not isotropic as was previously assumed.

3.3 Numerical Investigation

3.3.1 Overview

As discussed in the previous section, friction could have an influence on the vertical displacement of the probe during the swelling tests of the membrane. Numerical simulations have been performed to investigate this effect. For the simulations, the friction coefficient is varied from zero to 0.4 since the actual friction coefficient is unknown. After the effect of the friction is addressed, more simulations are performed to investigate the swelling behavior in both in-plane and out-of-plane direction and the simulation results are compared with the experimental results obtained in the above section. The hygrothermal conditions in the simulation are the same as those in the preliminary test. In this section, the models are briefly described.

3.3.2 Description of the Model

3.3.2.1 Out-of-plane Model

The commercial software ABAQUS 6.9 is used in this thesis to run the simulation. A two-dimensional axisymmetric model is constructed containing the probe, stage and proton exchange membrane (PEM) specimen as shown in Figure 3-6 to simulate the thickness swelling experiment. The material properties are assumed to be transversely isotropic with in-plane ($\epsilon_{xx}=\epsilon_{yy}$). both in-plane and out-of-plane swelling (ϵ_{zz}) behavior is given in the form of polynomial functions.

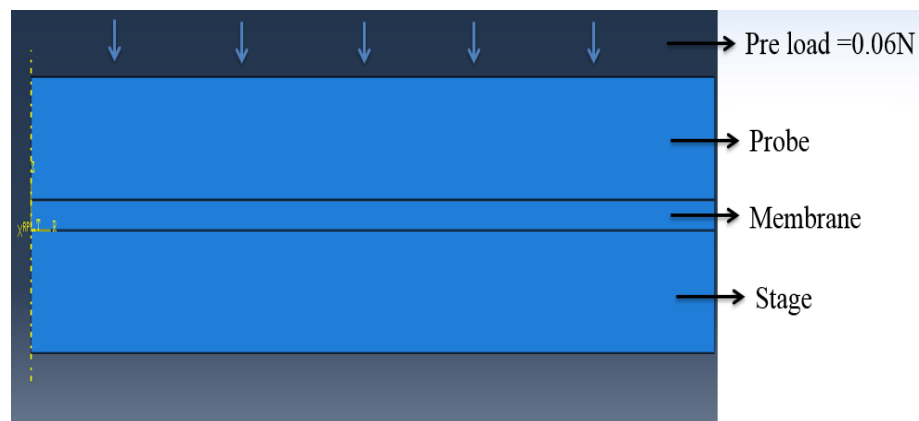


Figure 3-6 Schematic of numerical model for out-of-plane swelling coefficients investigation

3.3.2.1.1 Assumptions

The following assumptions are made in the numerical model:

- 1) In the model, the membrane is in contact with the stage and probe with friction in the tangent direction and hard (non-penetrating) contact in the normal direction. The friction is applied using the penalty approach.
- 2) The temperature and water content are uniform throughout the membrane and heat transfer and water diffusion is neglected in this simulation.
- 3) The boundary conditions, including temperature and humidity change are applied in a ramp-shaped time function.
- 4) Only the material properties of the membrane in the model are assumed to be dependent on temperature and humidity. While the material properties of the stage and probe don't change with hygro-thermal load.
- 5) The thermal expansion in this simulation is assumed to be isotropic and adopted from the previous work of former researchers [32].
- 6) The in-plane swelling and out-of-plane swelling are not coupled.

3.3.2.1.2 Boundary Conditions

For simplicity, both the temperature and humidity are applied to the whole membrane simultaneously, heat conduction and water diffusion are not considered. Eight-node, reduced integration coupled temperature-displacement, hybrid elements (CPEG8RHT)) are used for the out-of-plane simulation [58].

In the simulation, the membrane specimen is assumed to have the same initial size and shape (circular specimen with the same radius as the stage) as the probe and stage. For the stage, horizontal and vertical displacements, as well as rotation are constrained to be zero. For the probe, only vertical motion is allowed. The dimensional change due to temperature and humidity change is simulated. Five load steps, as shown in Figure 3-7 are included in the current simulation. The initial conditions represent the zero-stress state at room temperature and relative humidity, 25°C and RH=30%, in the example scheme. The entire hygrothermal cycles consist of the following 5 steps.

Step 1: Clamping: a fixed pressure is imposed on the top of the probe and held constant throughout the rest of the simulation. (This is to simulate the preload used to keep the probe in contact with the specimen in the experiments.)

Step 2: Temperature increase: Thermal-loading is achieved by linearly increasing the temperature to the desired value, (80°C in the example shown in Figure 3-7).

Step 3: Humidity Initialized: Hydro-loading is applied by linearly changing the water content to initial state (RH=25% in this example shown in Figure 3-7).

Step 4: Humidity Finalized: Hydro-unloading is achieved by linearly changing the RH to the desired value, (75% in the example shown in Figure 3-7).

Step 5: Humidity and temperature are kept at constant values until the entire system reaches steady state.

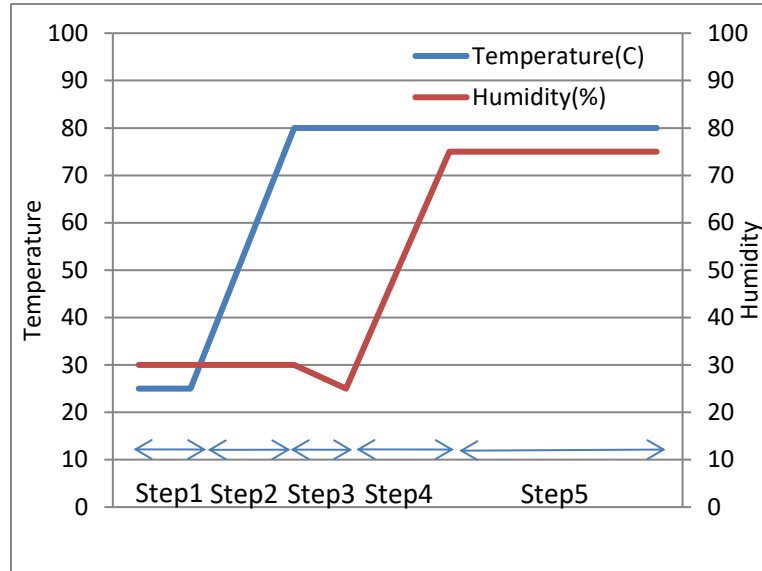


Figure 3-7 An Example of temperature and humidity cycle in the simulation

3.3.2.2 In-plane Model

A two-dimensional model is used to simulate the in-plane swelling test as shown in Figure 3-8. The membrane specimen is modeled as a generalized plane strain finite element model with a thickness of $30\mu\text{m}$ and length of $500\mu\text{m}$. The swelling behavior is assumed to be transversely isotropic with in-plane ($\epsilon_{xx}=\epsilon_{yy}$). Both in-plane and out-of-plane swelling (ϵ_{zz}) behavior is given in the form of polynomial functions.

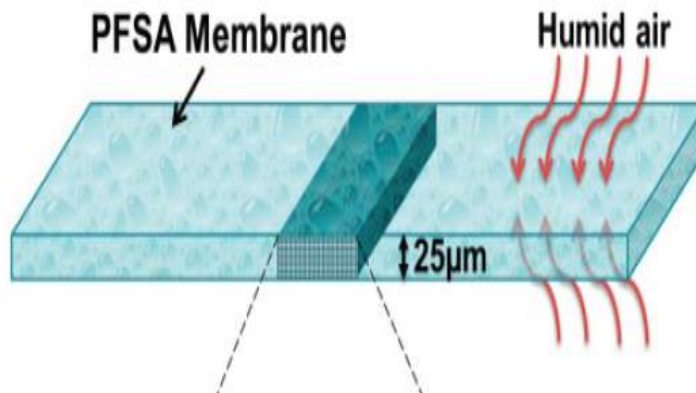


Figure 3-8 Schematic of numerical model for in-plane swelling coefficients investigation

3.3.2.2.1 Assumptions

The following assumptions are made in the numerical model:

- 1) The humidity is uniform within the membrane throughout the test and heat transfer and diffusion is neglected.
- 2) The in-plane swelling and out-of-plane swelling are not coupled.

3.3.2.2.2 Boundary Conditions

For the current simulation, both the temperature and humidity are applied to the whole membrane simultaneously, heat conduction and water diffusion are not considered. Eight-node, reduced integration coupled temperature-displacement, axisymmetric, hybrid elements are used for the out-of-plane simulation. The left edge is fixed and the right edge is constrained in the vertical direction and only allowed to move uniformly in the horizontal direction.

The loading steps applied in the in-plane test are identical to the steps mentioned in the out-of-plane simulation.

3.3.3 Material Properties

The material of the probe and stage used in the out-of-plane model described in Figure 18a is assumed to be quartz glass with Young's modulus=71.7 GPa and Poisson's ratio=0.17. The material properties of the probe and stage are assumed to be constant throughout the entire experiment: that is they don't expand or swell when temperature and humidity changes. The PFSA membrane used in both the in-plane and out-of-plane model is a time-dependent viscoelastic-plastic material and the mechanical properties, including the Young's modulus and Poisson's ratio have been determined by previous researchers in our lab [32, 39]. The PFSA membrane will experience hygro-thermal expansion during the test. The dimensional change of the membrane due to the hygro-thermal load is assumed to be anisotropic in the simulation. The total strain in the membrane due to temperature and humidity change is calculated from the coefficient of swelling and thermal expansion. And the in-plane and out-of-plane swelling behavior are given in the form of polynomial functions separately. The polynomial coefficients are then put into a subroutine to describe the hygro-thermal dimensional change when the environmental condition changes. The coefficients for in-plane swelling are given by the previous work by Kosuglu [18-20] and shown in Table 3-1a and the coefficients for the out-of-plane swelling, derived by fitting the out-of-plane swelling test results shown in Figure 3-5, are shown in Table 3-1b

C _{ij}	i=1	i=2	i=3	i=4
j=1	2.994E-12	-5.221E-10	3.574E-8	-6.832E-7
j=2	-4.303E-10	7.361E-8	-5.166E-6	1.003E-4
j=3	2.163E-8	-3.566E-6	2.564E-4	-5.067E-3
j=4	-5.402E-8	2.012E-5	-2.007E-3	4.355E-2

Table 3-1 (a) coefficient of in-plane swelling in terms of polynomial function [18]

C _{ij}	i=1	i=2	i=3	i=4
j=1	8.177E-12	-1.763E-9	1.085E-7	-1.889E-6
j=2	-1.907E-9	3.860E-7	-2.296E-5	3.921E-4
j=3	1.283E-7	-2.450E-5	1.432E-3	-2.396E-2
j=4	-2.153E-6	4.197E-4	-2.202E-2	3.410E-1

Table 3-1 (b) coefficient of out-of-plane swelling in terms of polynomial function

3.3.4 Results

To investigate the effect of friction on the simulation results, three different friction coefficients are studied, $F=0$ (frictionless), $F=0.2$ and $F=0.4$, and 3 probe clamping loads are selected, 0.06 N, 1.413N and 14.13N. The first one is the same as

the load in the preliminary test. The latter two correspond to 0.5MPa and 5MPa, which are typical compressive loads in the membrane in an operating fuel cell.

The out-of-plane stress fields for the 14.13N load and the various friction values are shown in Figure 3-9 a. It can be observed that when the friction is zero, the membrane is free to swell in the in-plane direction and therefore the stress is uniform throughout the membrane. However, when there is friction, the stress is no longer uniform and there is a stress gradient from the center of the specimen to the edge. This is because the friction acts as a “constraint” in the in-plane direction, which prevents the membrane from moving freely in the radial and tangential directions. Due to the axisymmetric geometry, the membrane at the center experiences greater constraint than the membrane at the outer edge. Therefore, when the temperature and humidity are increased, the membrane near the center swells more in the out-of-plane direction and less in the in-plane direction. As a consequence, the measured vertical displacement increases with increasing friction coefficient. This is in accordance with the displacement results shown in Figure 3-9c. When the applied force is large, 14.13N in this case, the displacement change during the hygro-thermal loading is sensitive to the friction.

The simulation also shows that the friction could have a strong influence on the results. From Figure 3-9 c, where the preload is 14.13N, when the friction coefficient changes from 0 to 0.2, the displacement change due to the hygrothermal loading increases by nearly 100%. However, the simulation indicates that the effect of the friction is small when the preload is small (Figure 3-9 b). It can be observed that when the loading is as low as 0.06N, which is the loading we applied in the TMA test, the differences in the displacements under the 3 different frictions conditions are

negligible. This is because when the normal load is small, even a large friction coefficient will not induce large frictional forces, so the constraint that prevents membrane swelling in the in-plane direction is negligible under these conditions. As a result, in the following numerical investigation, we assume the friction coefficient is 0.

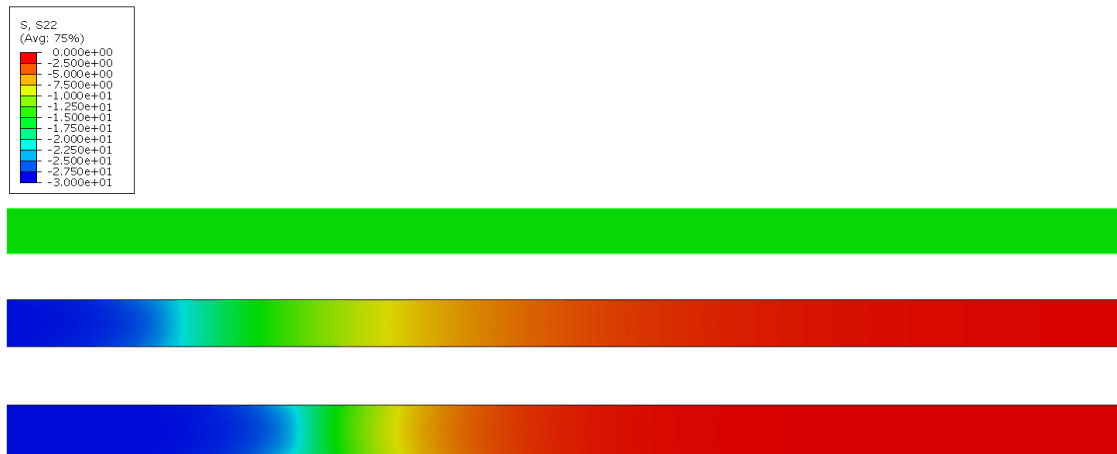


Figure 3-9 (a) Stress distribution in membrane under hygrothermal loading $F=14.13\text{N}$ with three friction coefficients a) $F=0$, b) $F=2$, c) $F=4$

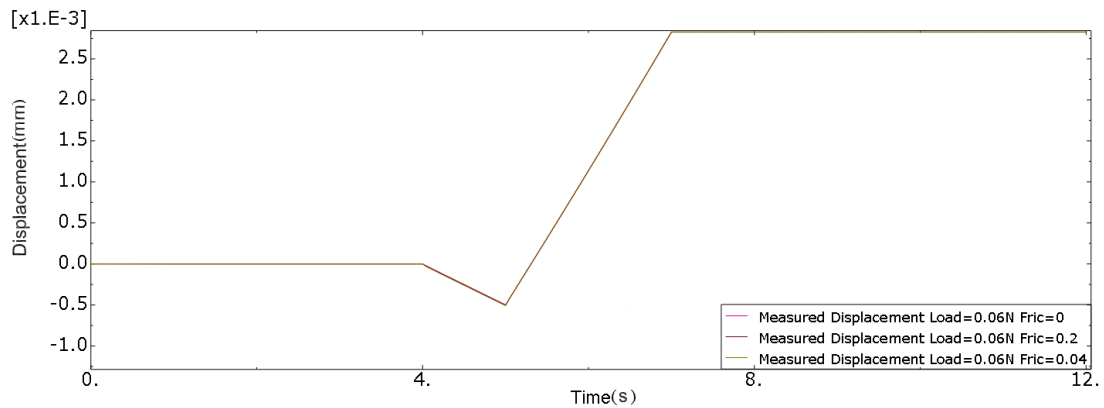


Figure 3-9 (b) Simulated out-of-plane displacement for model shown in Figure 3-6; Load=0.06N and with three friction coefficients

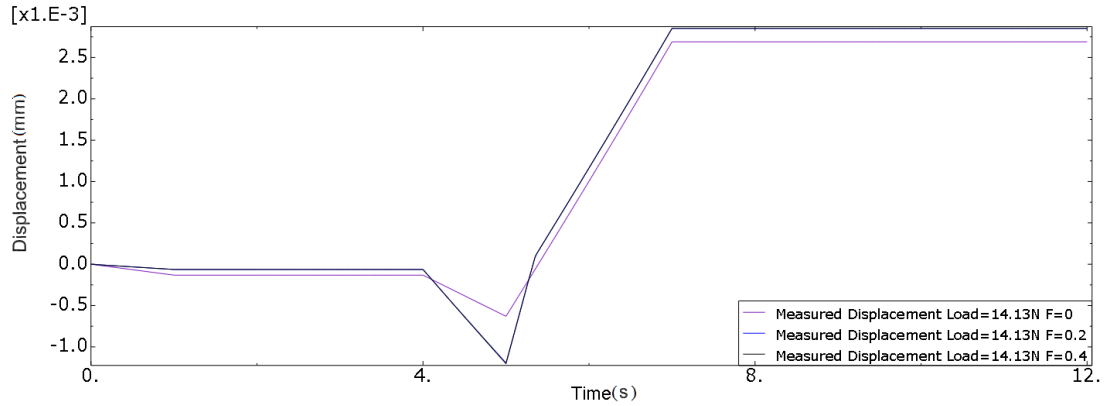


Figure 3-9 (c) Simulated out-of-plane displacement for model shown in Figure 3-6; Load=14.13N three friction coefficients

The results for the in-plane swelling using the numerical model in Figure 3-8 are shown in Figure 3-10. The in-plane swelling behavior of the membrane is described using the polynomial equation given in Table 3-1 a. With a 4th-order polynomial equation fit with 16 coefficients, the simulation results show a great match with the experimental data throughout the temperature and relative humidity combinations in this study.

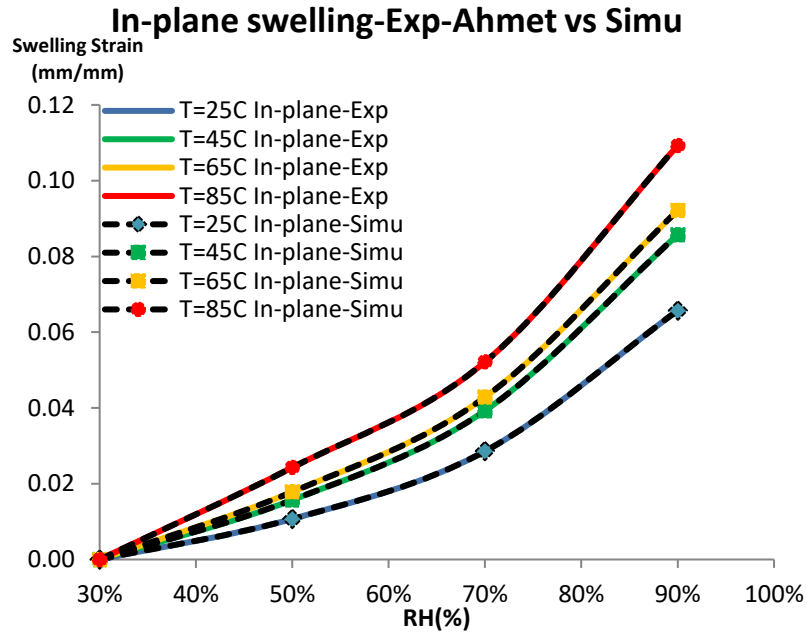


Figure 3-10 In-plane swelling using model Figure 3-8

The out-of-plane swelling behavior of the membrane is described using the polynomial equation given in Table 3-1 (b). The swelling coefficients are obtained through a least-square fit using the technical computing system Mathematica. Then the swelling equation is incorporated into the user-defined ABAQUS subroutine to simulate the out-of-the plane swelling of the membrane using the out-of-plane numerical model (shown in Figure 3-6). A gradient descent optimization iteration is used to obtain a better match between the experimental data and simulation results. The final coefficients for out-of-plane swelling are shown in Table 3-1 (b).

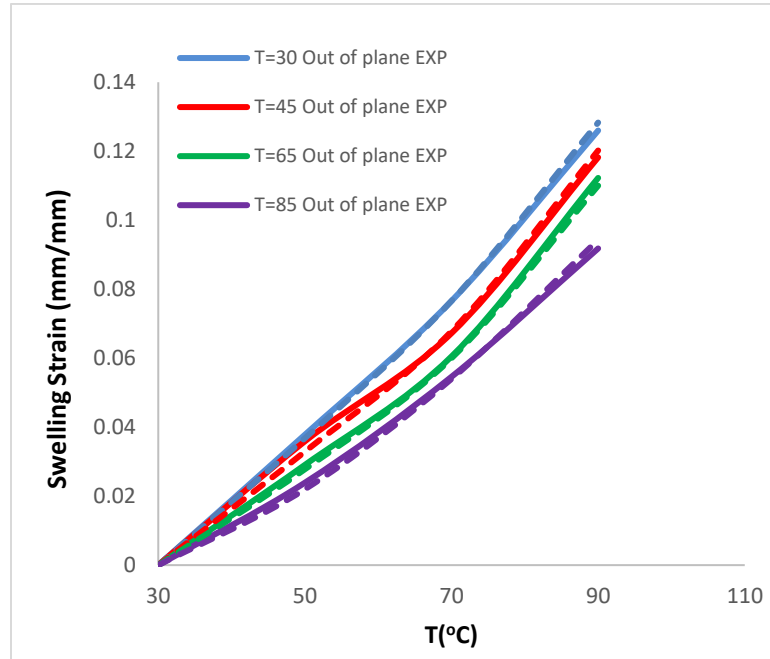


Figure 3-11 out-of-plane swelling using model Figure 18b

Figure 3-11 shows the simulation results using the axisymmetric numerical model. The swelling strain in the out-of-plane simulations results shows a great match with the experimental results. A slight difference is also observed (the maximum difference is less than 5%) in the figure. This difference could be due to the friction between the membrane and the platen. It is worth noting that this friction may vary with the relative humidity. When the humidity is high, liquid water could condense at the interface of membrane, causing the change in the friction coefficient, but in the current numerical model, we assume the contact between the membrane and probe/stage is frictionless. Another possible reason for the difference between experimental and simulation result could be attributed to the anisotropy of the mechanical properties of the membrane. In the current simulation, we assume the

Young's Modulus in the thickness direction is the same as that in in-plane direction, but this assumption might not be valid. From the previous test results obtained by Lu [30, 39], the Young's modulus of membrane in the in-plane direction is between 20 MPa and 400 MPa, depending on the loading rate, temperature and humidity. Assuming the out-of-plane modulus to be of a similar order of magnitude, the preload of 0.06N in the out-of-plane experiments could induce the strain in the order of 10^{-4} . Under this condition, the anisotropy of the mechanical properties of the membrane could lead to a noticeable difference in the strain. A third reason that could lead to the difference is that in the current simulation, the thermal expansion is assumed to be isotropic. Again, this assumption might not be valid for the current experiment.

3.4 Mechanical Response of PFSA Membranes under Hygrothermal Loading in Fuel Cell

In this part of the research, the effect of mechanical properties on the behavior of PFSA membranes in a fuel cell unit under RH and temperature cycling is studied by considering the anisotropic swelling of the membrane material. The simulations are conducted in a fuel cell numerical model developed by an earlier researcher in the lab. The detail of the model was described in Khattra's work [32] but repeated here for clarity. A sample model is illustrated in Figure 3-12.

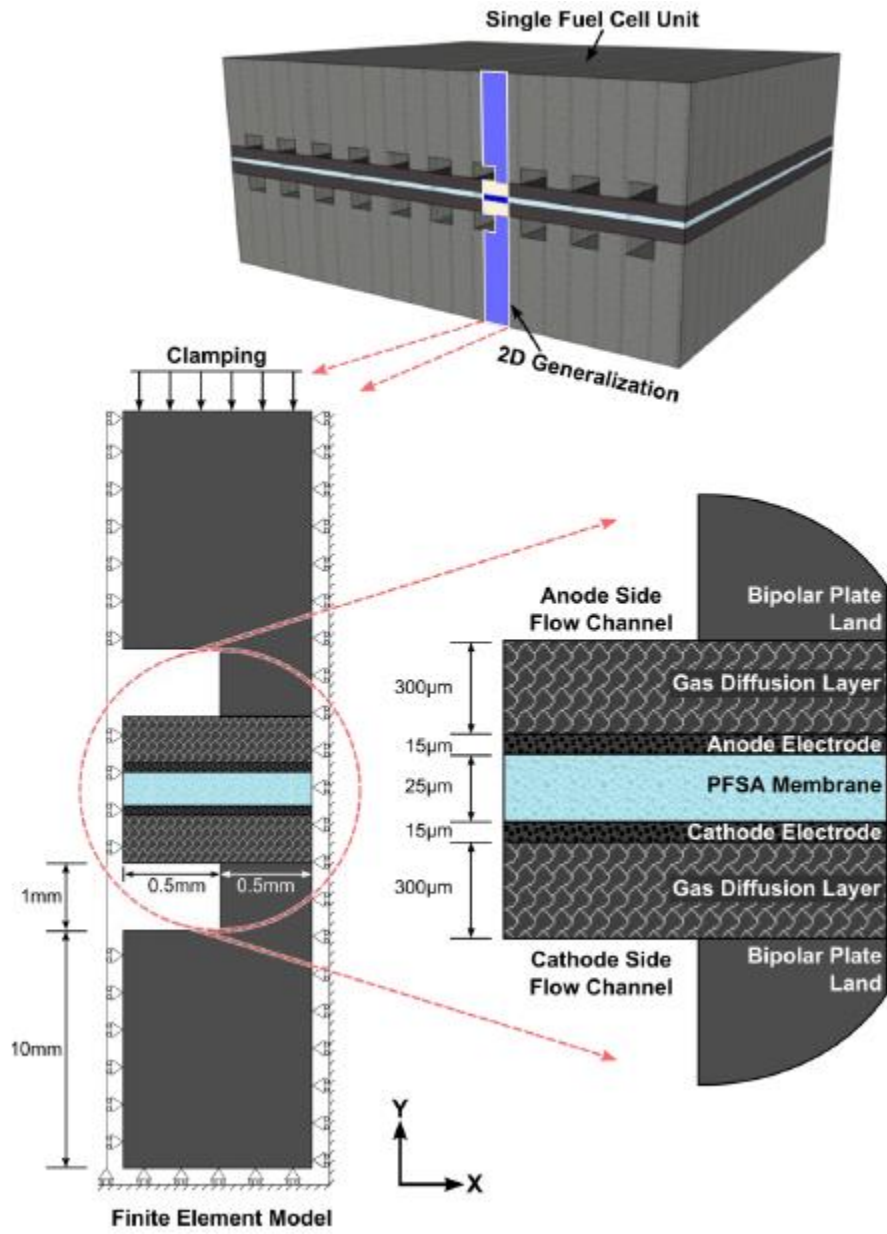


Figure 3-12 Schematic of the 2D generalization of fuel cell unit [32]

3.4.1 Material Properties

The material properties used in this simulation are described in the following section.

1. The bipolar plates are assumed to be linear-elastic with Young's modulus of 10GPa and Poisson's ratio of 0.25 [32]. The material properties of the bipolar plates are independent of temperature and humidity.
2. The porous, carbon-fiber gas diffusion layers (GDLs) are considered linear elastic and transversely isotropic with elastic modulus of 1500 MPa in the in-plane direction and 9 MPa out-of-plane and Poisson's ratio of zero [32]. The material properties of the GDLs are independent of temperature and humidity.
3. The electrodes, constructed with platinum-coated carbon PFSA, are assumed to be a viscoelastic-plastic material and their material properties are determined in Lu's research work [33].
4. The PFSA membrane is assumed to be a viscoelastic-plastic material and its mechanical properties are derived in previous work [17,18,32]. The viscoelastic-plastic material properties are assumed isotropic.
5. The swelling behavior of the membrane is considered anisotropic and the swelling coefficients are incorporated into the model by the polynomial fits described in the previous section.

3.4.2 Assumptions

The following assumptions are made in the finite element models:

Perfect bonding is assumed at the interfaces between components in the fuel cell. The mechanical response of all the components in the fuel cell is induced by changes in temperature and water content. In the current model, we didn't consider the

chemical reaction and neither heat generation nor water generation are considered in the model.

3.4.3 Boundary Condition

Two types of hygrothermal loading are applied to the fuel cell model.

A standard test procedure was developed by the US Department of Energy [2] to investigate the performance and durability of the membrane in fuel cell systems and this procedure is adopted in the current research and is referred to as “DOE cycle” in the following discussion. In the DOE cycle, the fuel cell starts from 25°C and is brought to a constant temperature of 80°C. The relative humidity (water content) is cycled on both the anode and the cathode sides of the membrane from 30% ($\phi=0.06$) to 100% ($\phi=0.32$). Each change of the humidity is applied in 1 sec ramp function in the simulation and after the change, the humidity is held constant for 120 sec

An alternative test procedure was developed by WL GoreTM [72] to study the mechanical durability of the membrane without considering the chemical reactions. It is similar to the DOE cycle mentioned above. It has the same start temperature and working temperature and the relative humidity (water content) also changes from 30% ($\phi=0.06$) to 100% ($\phi=0.32$) in a 1 sec ramp, as in the DOE cycle. The only difference is when the membrane is saturated, the RH is held constant for 10 sec before decreasing. When the dehydration is complete, the membrane is held in the dry condition for 50 sec before starting the next cycle.

3.4.4 Results and Discussion

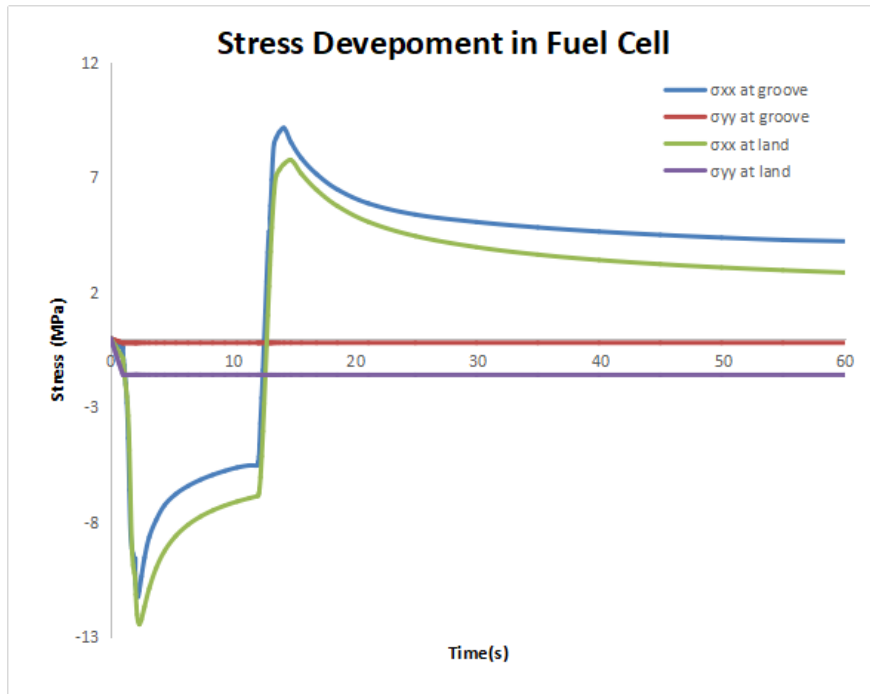
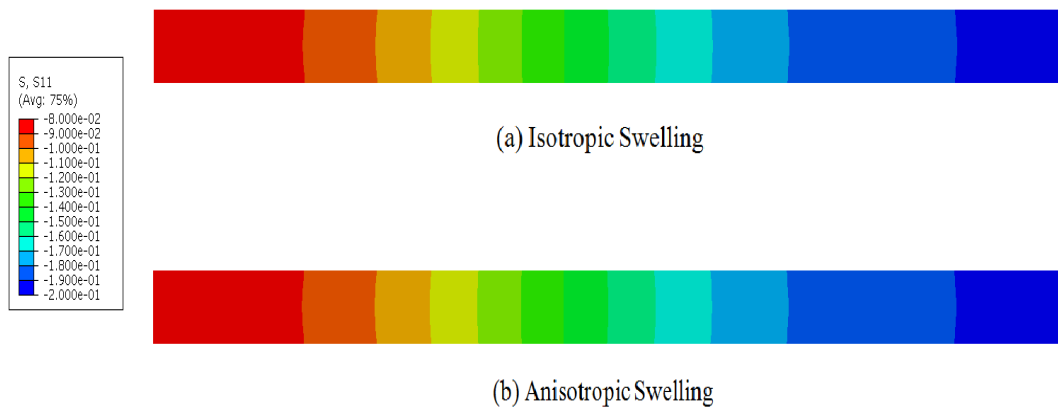


Figure 3-13 Development of the stress for elements in the membrane at the groove and the land side

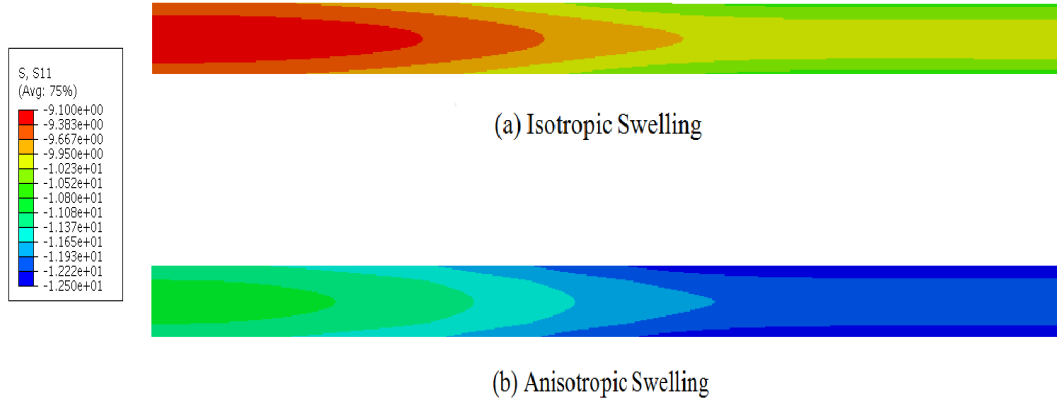
Figure 3-13 shows the in-plane and out-of-plane stress evolution at both the flow channel “groove” side and land side of the model (refer to Figure 3-12). Due to the geometry and the constraints in the fuel cell, the membrane experiences much larger in-plane stress as compared to the out-of-plane stress, which is consistent with the research of Khattri et al. [32] where the swelling of the membrane material is considered to be isotropic. Therefore, in the subsequent discussions we will concentrate on in-plane component of the stress. Meanwhile, since the mechanical degradation of the membrane in the fuel cell is more likely to take place in areas with

higher stress, we will focus on the groove side when comparing the stresses between the isotropic and anisotropic cases.

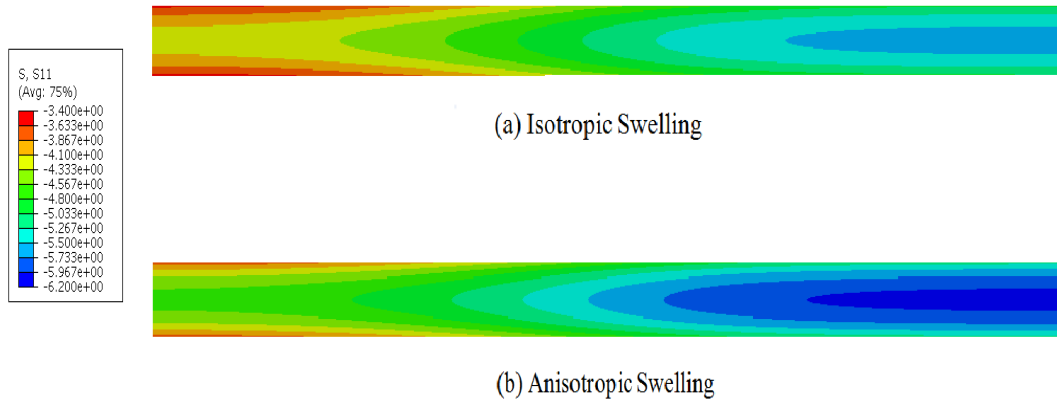
A) In-plane stress after clamping



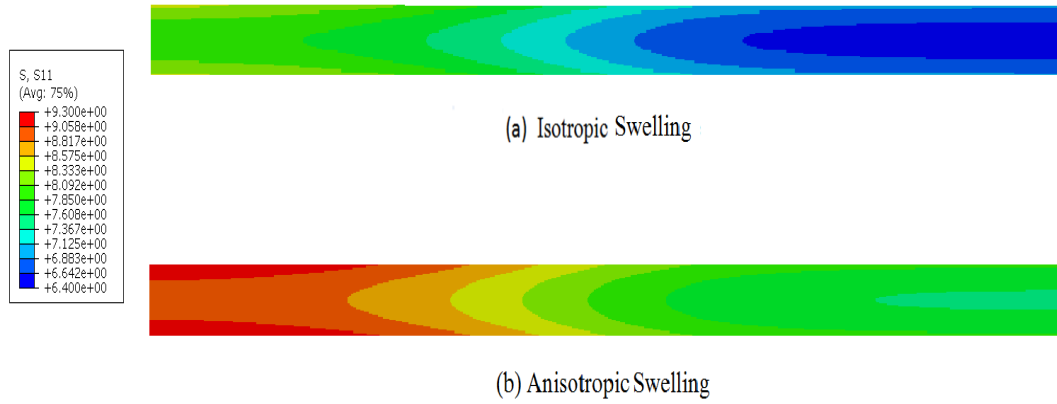
B) In-plane stress after hydration



C) In-plane stress at the end of hold at hydration



D) In-plane stress after dehydration



E) In-plane stress at end of hold at dehydration condition

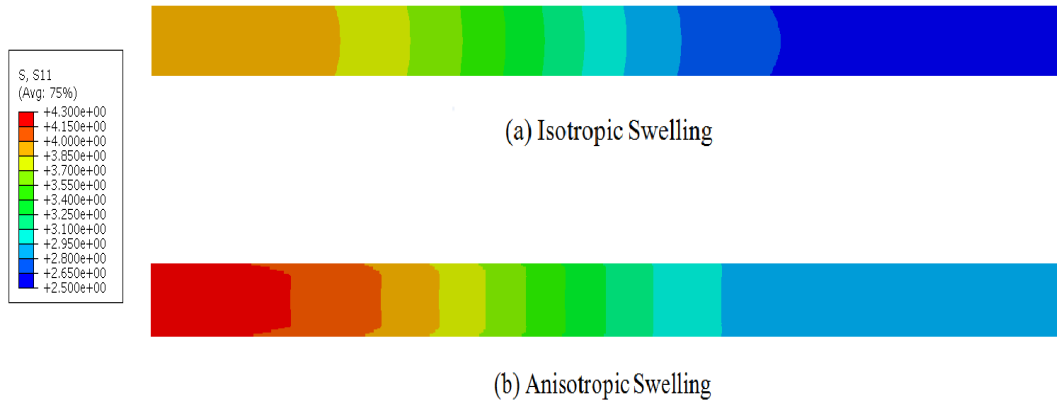


Figure 3-14 In-plane stress distribution contours (A-E) in the membrane during the first cycle of Gore™ RH load profile

Figure 3-14 shows the distribution of the in-plane stress contours for the membrane under the Gore temperature and RH cycle loading. The snapshots are marked A-E for the times corresponding to the end of clamping, hydration, hydration-hold, dehydration and dehydration-hold times respectively. In each figure, the stress magnitude and distribution are compared between isotropic membrane swelling (previous results of Khattra et al. [32]) and anisotropic membrane swelling described in the previous chapter (refer to chapter 3.2 and chapter 3.3).

From Figure 3-14 A, we can see there is a small compressive stress throughout the membrane after initial clamping. The stress is uniform through the thickness and increases in the in-plane direction from groove to land. Since there is no membrane swelling at this point, the stress distribution and magnitude are the same for both isotropic and anisotropic cases. As the start point, the membrane has relative humidity of 30% ($\phi=0.06$) and temperature of 25°C.

The membrane is then heated up to 80°C as the working temperature and hydrated to a relative humidity (water content) of 100% ($\phi=0.32$). This change of the boundary condition is applied in a ramp function, over a time period of 1 sec. The increase of temperature and relative humidity causes thermal expansion and hygro-thermal swelling in the membrane. At the same time, the membrane becomes less stiff and its proportional limit decreases due to its temperature and water-content dependent material properties (see [29, 32]). The membrane cannot expand or swell freely due to the constraint from other components of the fuel cell such as the bipolar plates and GDLs. Therefore, a relatively large compressive stress develops in the membrane (Figure 3-14 B). The stress distribution is similar for both isotropic and anisotropic simulations but the stress magnitude is much larger for the anisotropic case. The

maximum stress increased by 16.8%. This is due to the out-of-plane swelling coefficient being larger than the in-plane swelling coefficient. Consequently, the incorporation of swelling anisotropy induces more compressive stress in the membrane.

The high humidity (water content) 100% ($\phi=0.32$) is held in the membrane for 10 sec (Figure 3-14 C). During this time, the magnitude of the compressive stress decreases and the stress redistributes throughout the membrane (Figure 3-14 C) due to the visco-elastic behavior of the membrane. The stress distribution is similar for both isotropic and anisotropic simulations and again the magnitude is larger for the latter case. But the difference of the maximum stress magnitude decreases to about 7% at this point in the cycle. We can see from the results that as the stress redistributes, not only the maximum stress decreases, but also the difference between the maximum stress in the isotropic and anisotropic cases decreases.

The membrane is then dehydrated to a relative humidity (water content) of 30% ($\phi=0.06$), which causes the membrane to shrink and increases the stiffness and proportional limit. A relatively large tensile stress develops in the membrane (Figure 3-14 D). This is because during hydration, the compressive stress in the membrane was large enough to lead to plastic deformation. When the relative humidity decreases, the membrane shrinks. As mentioned above, the membrane is perfectly constrained by the other components of the fuel cell, so a residual tensile stress can develop in the membrane. Holding the membrane in the dry state for 50 sec results in tensile stress relaxation and redistribution as shown in (Figure 3-14 E). The stress distribution is similar for both isotropic and anisotropic simulations and again, the magnitude is larger for the latter case.

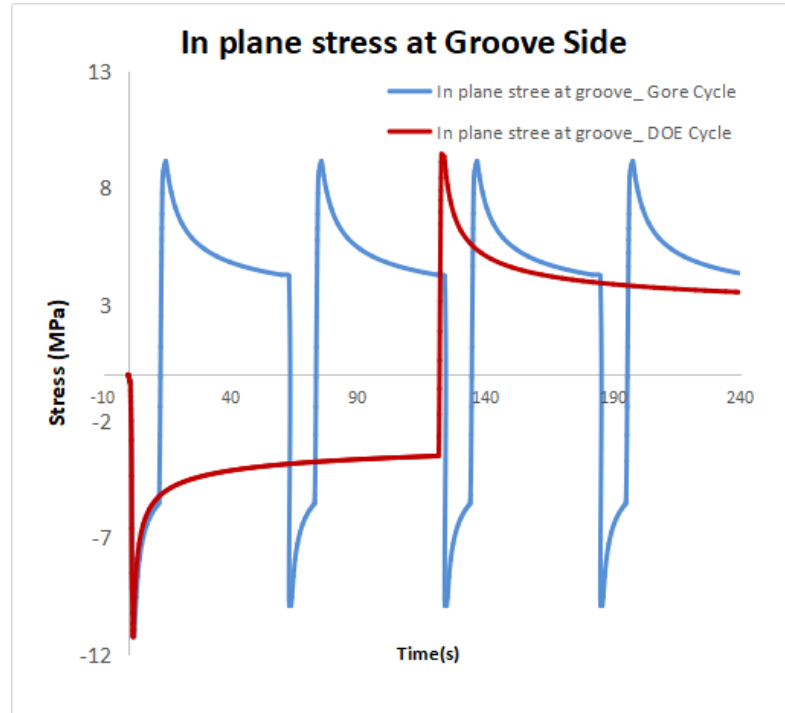


Figure 3-15 Evolution of the in-plane stress at Groove Side

The evolution of the in-plane stress with time is shown in Figure 3-15. From Figure 3-13, we can see that the maximum residual tensile stress occurs on the groove side and the spot with maximum residual tensile stress is the place where the mechanical degradation is most likely to occur. As a result, we focus on the groove side in this discussion.

The stress evolution in the membrane is compared between results from a Gore RH cycle and DOE cycle simulation using viscoelastic-plastic properties and anisotropic swelling property in Figure 3-15. From the figure, we can see in the DOE

RH cycle, the stress range is about 1.1% larger than in the Gore RH cycle and the maximum tensile stress in the DOE cycle is about 2.5% more than in the Gore cycle. This could be attributed to the fact that for the DoE cycle, the strain is kept constant for longer time, which leads to a longer relaxation of the membrane. However, the Gore cycle produces a greater number of cycles (in this case, 4 times more cycles) for a given test period.

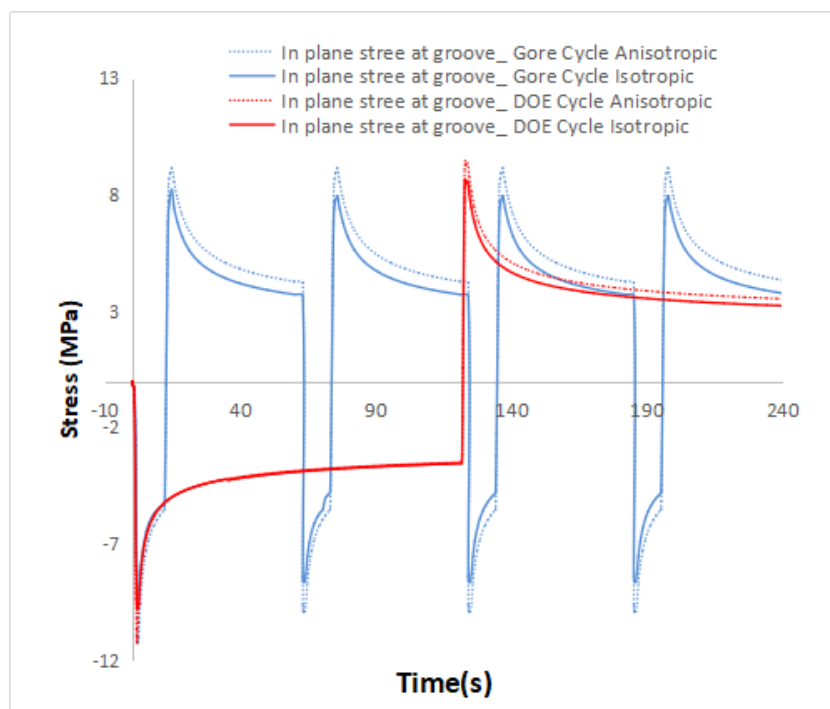


Figure 3-16 Evolution of the in-plane stress for isotropic and anisotropic case

The evolution of the in-plane stress for the isotropic and anisotropic cases are shown and compared in Figure 3-16. For the Gore cycle, the introduction of the anisotropic swelling increases the stress range by 13.2% and increases the maximum

residual tensile stress by 11.2%. For the DoE cycle, by considering the anisotropic swelling, the stress range throughout the hygrothermal loading increases by 12.4% and the maximum tensile stress increases by 9.2%. We can see that if we incorporate the anisotropic out-of-plane swelling into the current model, the difference in stress between Gore cycle and DoE cycle becomes less significant.

3.5 Summary

Experiments and numerical simulations are performed to investigate the out-of-plane mechanical behavior of PFSA membrane under various temperature and humidity combinations. The experiment shows that the swelling behavior of the membrane under hygrothermal loading is not isotropic. The anisotropy of the swelling is more significant when the temperature is low. The swelling in the out-of-plane direction is generally larger than that in the in-plane direction. Specifically, the swelling of the membrane increases with the relative humidity. However, unlike the swelling behavior at in-plane direction, the swelling at the out-of-plane direction decreases with increasing temperature. At 85°C the swelling coefficient in the out-of-plane direction is close to the coefficient in the in-plane direction, while at 25°C, the swelling coefficient in the out-of-plane direction is much larger than the coefficient in the in-plane direction. The measured swelling behavior is described using a polynomial curve-fitting equation and the coefficients of the equation are obtained through a set of numerical simulations. Then the swelling of the membrane is incorporated into a fuel cell stack numerical model to have better insight into the development of stress during fuel cell operation. According to the simulation results,

by considering the anisotropic out-of-plane swelling, the stress distribution and stress history in the fuel cell change significantly. The residual in-plane stresses still dominant and the maximum stress still occurs at the groove side of the fuel cell. However, the magnitude of the stress increases by as much as 12.4% using the DoE relative humidity cycle, indicating that the fuel might undergo larger residual stress and the anticipated lifetime of the fuel might be less if we take the anisotropy of the membrane swelling into consideration.

Chapter 4

CONCLUSIONS AND FUTURE WORK

4.1 Summary of Work

The durability of PEMFCs has been a critical obstacle to the commercialization of fuel cells and the durability of the PFSA membrane usually determines the lifetime of the whole cell. A number of studies have been performed in recent years and these studies have revealed that mechanical and chemical degradation are the two main factors that contribute to the failure of the fuel cell membrane [1, 5]. The change of the temperature and relative humidity during the fuel cell operation causes expansion and shrinkage of the membrane, resulting in mechanical stresses in the membrane. The stresses, according to the previous research [32], are the primary driver of the mechanical damage. This work is aimed at understanding the mechanical response of the membrane under hygrothermal loading. Fatigue testing was performed to characterize and understand the failure behavior of the membrane and its dependence on the environmental conditions. The effect of anisotropic swelling behavior of the membrane is also studied. The swelling characterization in the out-of-plane direction is measured in a customized TMA test machine and the test results are incorporated in a numerical model to investigate the mechanical response of the membrane in the fuel cell stack.

The following is the summary of the research and conclusions drawn from this work.

Fatigue on the PFSA membrane: Fatigue tests are performed on Nafion® 211 membrane to understand the failure mechanism and to predict the durability of the PFSA membrane. The results show that both mechanical and hygrothermal load have an influence on the fatigue life of PFSA membrane. The fatigue life of the membrane decreases when the applied stress is larger. When the mechanical load and temperature are constant, the crack propagation rate increases exponentially with the relative humidity, When the humidity and applied load are kept as constant, the crack propagation rate increases substantially with increasing the temperature. Moreover, when the temperature and relative humidity decrease below a certain level at a given load, for example, $T=25^{\circ}\text{C}$ $\text{RH}=50\%$ under our selected fatigue load, the crack in the membrane stops propagating or propagates at a significantly small rate, which indicates the membrane has an apparent fatigue limit, below which fatigue failure doesn't occur.

Swelling behavior of the membrane at out-of-plane direction: The swelling behavior of the membrane is a function of hygrothermal loading. More specifically, it depends on the temperature and relative humidity. The current work shows that the swelling of the membrane under hygrothermal loading is not isotropic as previously assumed. In the out-of-plane direction, the swelling of the membrane increases with increasing relative humidity but decreases with increasing temperature. The swelling coefficient in this direction is larger than that in the in-plane direction for almost all temperatures, but the difference is more significant when the temperature is low. The out-of-plane and in-plane swelling behavior are described using polynomial equations incorporated into a fuel cell numerical model. By considering the anisotropy of the swelling of the membrane, the stress distribution and stress history in the fuel cell

changes significantly but the spot where maximum compressive and tensile stresses occur remains the same when compared with the case where the material is assumed to be isotropic. For the GoreTM RH cycle, the stress range increases by 13.2% and the maximum residual tensile stress increases by 11.2%. For the DoE RH cycle, the stress range increases by 12.4% and the maximum residual tensile stress increases by 9.2%. These results indicate that the lifetime prediction from an isotropic swelling model might be longer than the in the case where the swelling anisotropy in the membrane is considered.

In summary, this thesis work was conducted to study the mechanical response and characterizing of the PFSA membrane through a mixture of experimental and numerical methods. In particular, we studied the fatigue behavior of the membrane through experiment investigation, where we applied cyclic loading to a pre-cracked Nafion® 211 membrane sample under various environmental conditions. We also studied the anisotropy of the swelling of the membrane by performing tests in a TMA test facility and incorporating the swelling behavior into a numerical fuel cell model to characterize the mechanical response of the membrane in fuel cell operation. The findings in this research work provide a better understanding of the mechanical properties of PFSA membrane and its mechanical response in the fuel cell system. This will help provide better insight into the failure mechanisms of the fuel cell and provide more reliable tools to predict the lifetime of the fuel cell.

4.2 Future Considerations

Improvements to this work can be realized by further investigating the assumptions we made in the current research. In this work, we made some simplifying

assumptions in the simulation. For example, in the out-of-plane swelling coefficient test, we assumed the friction between the membrane and test facilities is negligible. We also assume that the mechanical properties, including the Young's modulus and yield stress are isotropic. These assumptions need further investigation.

In the current work, the swelling behavior of the membrane is characterized and incorporated into the numerical model using a polynomial equation. This approach cannot provide insight into the swelling mechanism of the membrane and its relationship with temperature and relative humidity. As a result, a constitutive relation that implements both temperature and relative humidity could be developed to better describe the swelling behavior of the membrane in phenomenological terms. Beyond that, a micro-structure model of the membrane that can capture the out-of-plane swelling behavior of the membrane can be developed to further enhance understanding and predictive capabilities.

Chemical deterioration of the membrane properties is not considered in the current numerical model of the membrane. Even though mechanical degradation is one of the important factors that contribute to the failure of the fuel cell, the chemical degradation is also an important factor. For example, during the fuel cell operation, the electrodes and the membrane might wear away due to chemical degradation so that the geometry and the boundary conditions that confine the fuel cell membrane could change. To account for this deterioration of the material, a chemically-mediated damage mechanism might be added to the finite element model. In this case, a dynamic meshing method might be needed to account for the changes in geometry and boundary conditions during the simulation.

Moreover, our current 2-D model cannot simulate the ex-situ fatigue test very accurately since out-of-plane wrinkling or buckling near the crack tip cannot be simulated in the current model. To better simulate the fatigue test, a 3-D model needs to be developed. Meanwhile, the cyclic load will be applied thousands of time on the PFSA membrane before it breaks (see Figure 2-7 to Figure 2-9). It is very time consuming and computationally expensive to run the simulation with so many cycles. As a result, some accelerated simulation techniques need to be developed.

REFERENCES

- [1] W. R. Grove, *Philosophical Magazine* 3, 127-130 (1839).
- [2] J. Milliken, DOE Hydrogen Program 2008 Annual Progress Report, U. S. Department of Energy, 2008
- [3] L. Carrette, K.A. Friedrich, U. Stimming, *Fuel Cells - fundamentals and applications* 1 (2001) 5-39.
- [4] R. J. Farrauto, *Science and Technology in Catalysis*, 145, 21-29 (2003)
- [5] R. Borup, J. Meyers, *Chemical Reviews*, 107, 3904-3951 (2002).
- [6] N. L. Garland, J. P. Kopasz, *Journal of Power Source*, 172, 94-99 (2007)
- [7] U. Beuscher, S.J.C. Cleghorn, *International Journal of Energy Research*, 29, 1103-1112 (2005)
- [8] S. Cleghorn, J. Kolde, *Handbook of Fuel Cells Fundamentals, Technology and Applications*, John Wiley & Sons, Ltd, (2003)
- [9] J. Xie, D.L.W. III, *Journal of the Electrochemical Society*, 152, 104-113 (2005)
- [10] S. Kundu, M.W. Fowler, *Journal of Power Sources*, 157, 650-656 (2006)
- [11] P. Rama, R. Chen, *Proceedings of the Institution of Mechanical Engineers, Part A: Journal of Power and Energy*, 222 421-441 (2008)
- [12] M. Crum, W. Liu, *Electrochemical Society Inc.*, 2006, 541-550.
- [13] D.A. Dillard, M. Budinski, *Proceedings of the 3rd International Conference on Fuel Cell Science, Engineering, and Technology*, Ypsilanti, MI, United States, 153-159 (2005)
- [14] J. W, X. Y, J. J. Marin, *Journal of Power Source*, 184, 104-119 (2008)

- [15] J. Healy, C. Hayden, T. Xie, K. Olson, R. Waldo, M. Brundage, H. Gasteiger, J. Abbott, *Fuel Cell*, 5, 302-308 (2005)
- [16] A. Kusoglu, A.M. Karlsson, M.H. Santare, S. Cleghorn, W.B. Johnson, *Journal of Power Sources*, 161, 987-996 (2006)
- [17] Y. Tang, M.H. Santare, A.M. Karlsson, S. Cleghorn, W.B. Johnson, *Journal of Fuel Cell Science and Technology*, 3, 119-124 (2006)
- [18] Y. Tang, A.M. Karlsson, M.H. Santare, M. Gilbert, S. Cleghorn, W.B. Johnson, *Journal of Material Science*, 425, 297-304 (2006)
- [19] A. Kusoglu, A.M. Karlsson, M.H. Santare, S. Cleghorn, W.B. Johnson, *Journal of Power Sources*, 170, 345-358 (2007)
- [20] A. Kusoglu, A.M. Karlsson, M.H. Santare, S. Cleghorn, W.B. Johnson, *ECS Transactions*, 16, 551-561 (2008)
- [21] Y. Tang, A. Kusoglu, A.M. Karlsson, M.H. Santare, S. Cleghorn, W.B. Johnson, *Journal of Power Sources*, 175, 817-825 (2008)
- [22] Thermo Mechanical Analysis Manual Book.
- [23] C. Xia, F. Chen, M. Liu, *Electrochemistry*, 4, 52-54 (2001)
- [24] B. C. H. Steele, A. Heinzl, *Nature*, 414, 345-352 (2001)
- [25] G. A. Eisman, *Proceedings of the 168th Electrochemical Society*, 86, 156-171 (1986).
- [26] Y. Tang, A. M. Karlsson, *Material Science and Engineering*, 425, 297-304 (2006)
- [27] Costamagna, P., and Srinivasan, S., 2001, *Journal of Power Sources*, 102(1-2), pp. 253-269.
- [28] Kolde, J. A., and Bahar, B., *Proc. Electrochemical Society Proceedings*, pp. 193-201.
- [29] Merlo, L., Ghielmi, A., Cirillo, L., Gebert, M., and Arcella, V., 2007, 42(13), pp. 2891-2908.
- [30] Z. Lu, M. Lugo, *Journal of Power Source*, 214, 130-136, (2012)

- [31] A. Z. Weber, J. Newman, *Aiche Journal*, 50, 3215-3226 (2004)
- [32] N. S. Khattrra, Ph.D. Dissertation, University of Delaware, 2012
- [33] Z. Lu, C. Kim, A. M. Karlsson, J. C. Cross III, M. H. Santare, *Journal of Power Source*, 196, 4646-4654 (2011)
- [34] R. Solasi, Y. Zou, X. Y. Huang, K. Reifsnider, *Mechanics of Time-Dependent Materials*, 12, 15-30 (2008)
- [35] M. N. Silberstein, M. C. Boyce, *Journal of Power Sources*, 195, 5692-5706 (2010)
- [36] Y. H. Lai, C. K. Mittelsteadt, C. S. Gittleman, D. A. Dillard, *Journal of Fuel Cell Science and Technology*, 6, 13 (2009)
- [37] T.T. Aindow, J. O'Neill, *Journal of Power Sources*, 196 (2011) 3851-3854
- [38] M. N. Silberstein, P. V., Pillai, M. C. Boyce, *Polymer*, 52, 529-539 (2011)
- [39] Z. Lu, 2012, Ph.D. Dissertation, University of Delaware, 2012
- [40] A. Kusoglu, M.H. Santare, A.M. Karlsson, S. Cleghorn, W. B. Johnson, *Journal of Electrochemical Society* 157, 705-713 (2010)
- [41] A. Kusoglu, M.H. Santare, A.M. Karlsson, *Polymer*, 50 2481-2491(2009)
- [42] Y. Singh, R.M.H. Khorasany, *International Journal of Hydrogen Energy* 42 (2017) 19257-19271
- [43] Goulet MA, Khorasany RMH, *J Power Sources* 2013, 234-247.
- [44] Goulet M, Arbour S, Lauritzen M, Kjeang E. *J Power Sources* 2015, 274-286.
- [45] Khorasany RMH, Sadeghi Alavijeh A, Kjeang E, *J Power Sources* 2015, 274,1208-1224.
- [46] A. Kusoglu, M.H. Santare, A.M. Karlsson, S. Cleghorn and W. B. Johnson, *Journal of Polymer Science*, 46, 2404-2417 (2008)
- [47] A. Kusoglu, A.M. Karlsson, M.H. Santare, *Polymer*, 51, 1457-1464 (2010)

- [48] T. M. Keaveny, E. F. Wachtel, C. M. Ford, W. C. Hayes, *Journal of Biomechanics*, 27, 1137-1146 (1994)
- [49] W. Y. Hsu, T. D. Gierke, *Journal of Membrane Science* 13, 307-326 (1983)
- [50] W. Y. Hsu, T. D. Gierke, *Journal of Membrane Science* 13, 307-326 (1983)
- [51] J. Y. Li, S. Nemat-Nasser, *Mechanics of Material*, 32, 303-314 (2000)
- [52] Y. Benveniste, *Mechanics Research Communication*, 13, 193-201 (1986)
- [53] D. B. Lanning, T. Nicholas, G. K. Haritos, *International Journal of Fatigue*, 27, 45-57 (2005)
- [54] T. Mataka, *Bulletin of the JSME*, 141, 257-263, (1977)
- [55] Kurkoski, S.M. Senior thesis, University of Delaware 2014
- [56] M. Pestrak, Y. Li, *Journal of Fuel Cell Science and Technology*, 7 (2010) 41009.1-041009.10
- [57] Y. Kai, Y. Kitayama, *Journal of Fuel Cell Science and Technology*, 10 (2013) 021007.1-21007.8
- [58] ABAQUS. ABAQUS Analysis User's Manual, 2010.
- [59] D. A. Brune, J. Bicerano, *Polymer*, 43, 369-387 (2002)
- [60] Sadeghi Alavijeh A, Khorasany RMH, Habisch A, *J Power Sources* 2015, 285-268.
- [63] E. Andrews, W. Sanders, L.J. Gibson, *Material Science and Engineering: A*, 270, 113-124 (1999)
- [65] The V-Gen™ Dew Point/RH Generator, InstruQuest Inc.
- [66] W. Chen, F. Lu, M. Cheng, *Polymer Test*, 21, 113-121 (2002)
- [67] Y Lai, D Dillard, A Vielstich, H Gasteiger, H Yokokama. *Handbook of Fuel Cells Volume 5: Advances in Electrocatalysis, Materials, Diagnostics and Durability*. John Wiley & Sons, 2009.

- [68] S Burlatsky, M Gummalla, J O'Neill, Journal of Power Sources, 215 (2012) 135-144.
- [69] R Banan, J Zu, A Bazylak. Fuel Cells, 15 (2015) 327-336.
- [70] Qiang Lin, Shouwen Shi, Journal of Power Sources Volume 384, 30 April 2018, Pages 58-65
- [71] Zhe Zhang, Shouwen Shi, International Journal of Hydrogen Energy (2018), 6379-6389
- [72] W Liu, S Cleghorn. ECS Transactions, 1 (2006) 263-273.